**Forschungszentrum Karlsruhe**
in der Helmholtz-Gemeinschaft

**Wissenschaftliche Berichte**
FZKA 7364

# Physical Chemistry of Corrosion and Oxygen Control in Liquid Lead and Lead-Bismuth Eutectic

**C. Schroer, J. Konys**

**Institut für Materialforschung**
**Programm Nukleare Sicherheitsforschung**

**Dezember 2007**

**Forschungszentrum Karlsruhe**

in der Helmholtz-Gemeinschaft

Wissenschaftliche Berichte

FZKA 7364

# Physical Chemistry of Corrosion and Oxygen Control in Liquid Lead and Lead-Bismuth Eutectic

Carsten Schroer, Jürgen Konys

Institut für Materialforschung

Programm Nukleare Sicherheitsforschung

Forschungszentrum Karlsruhe GmbH, Karlsruhe

2007

Forschungszentrum Karlsruhe GmbH
Postfach 3640, 76021 Karlsruhe

Mitglied der Hermann von Helmholtz-Gemeinschaft
Deutscher Forschungszentren (HGF)

ISSN 0947-8620

urn:nbn:de:0005-073648

## Abstract

Corrosion of steel in liquid lead (Pb) and lead-bismuth eutectic (LBE) is an important factor when applying these materials as a process medium. At low oxygen content of the liquid-metal phase, the degradation results mainly from the dissolution of the steel constituents, which may significantly decrease in the presence of a continuous scale of oxides of the steel constituents on the steel surface. In order to facilitate the formation of such a scale, the oxygen content of the liquid metal has to be controlled. Therefore, a method of measuring the oxygen content must be available. This report addresses the thermodynamic fundamentals of steel corrosion in oxygen-containing liquid metals and provides the data on chemical and physical properties which is required for the determination of favourable conditions with respect to the oxygen content and the numerical analysis of the dissolution of the primary steel constituents in oxygen-containing liquid Pb and LBE. Furthermore, the measurement of the oxygen content with electrochemical oxygen sensors and the evaluation of the sensor output is discussed.

## Kurzfassung

### Physikalische Chemie der Korrosion und Kontrolle des Sauerstoffgehaltes in flüssigem Blei und eutektischem Blei-Bismut

Ein wesentliches Problem beim Einsatz von flüssigem Blei (Pb) bzw. eutektischem Blei-Bismut (LBE) als Prozessmedium ist die Korrosion von Stählen durch Auflösung der Stahlbestandteile. Diese lässt sich prinzipiell dadurch mindern, dass über die Zugabe von Sauerstoff die Bildung einer schützenden Schicht von Oxiden der Stahlbestandteile auf der Stahloberfläche angeregt wird. Um den Verbrauch des Sauerstoffs durch die Oxidbildung auszugleichen, ist eine ständige Kontrolle erforderlich, was ein geeignetes Verfahren zur Messung des Sauerstoffgehaltes voraussetzt. Im vorliegenden Bericht werden die thermodynamischen Grundlagen der Stahlkorrosion in sauerstoffhaltigen Flüssigmetallen erörtert und Stoffdaten zusammengefasst, die zur Bestimmung geeigneter Bedingungen hinsichtlich des Sauerstoffgehaltes sowie zur theoretischen Behandlung der Auflösung der Hauptbestandteile von Stählen in sauerstoffhaltigem Pb bzw. LBE erforderlich sind. Des Weiteren werden die Messung des Sauerstoffgehaltes mit elektrochemischen Sauerstoffsonden und die Auswertung der Sondensignale behandelt.

# Table of contents

# 1 Introduction

The performance of steels in liquid metals strongly depends on the presence of oxygen dissolved in the liquid metal phase. If the oxygen content exceeds a certain threshold, a continuous scale consisting of oxides of the steel constituents may form on the steel surface separating the steel from the liquid metal. Consequently, the dissolution of steel constituents, which is the main degradation mechanism at low oxygen content of the liquid-metal phase, can occur only after diffusion through the oxide scale, i.e., at a potentially lower rate. Additionally, the maximum concentration of steel constituents dissolved in the liquid metal decreases when oxides of the steel constituents are stable, as follows from the respective solubility products. The efficiency of the oxide scale with respect to the reduction of material degradation is influenced by the composition and especially by the structure of the scale, with the optimum being a slow growing scale allowing only low diffusion rates of the steel constituents. Oxygen is steadily consumed by the formation of oxides on the steel surface; therefore, the oxygen content of the liquid metal has to be controlled via appropriate oxygen probes and a method of adding oxygen to the liquid metal. The reduction of steel corrosion by addition of oxygen is only applicable, if at least one of the steel constituents is less noble than the components of the liquid metal, and the concentration of less-noble steel constituents has to be sufficiently high to form a continuous oxide scale on the steel surface.

Which oxides of the steel constituents are thermodynamically stable and may form on the steel surface, is determined by the chemical potential or the activity of oxygen in the liquid metal. Hence, the knowledge of the oxygen potential/activity, e.g., from measurements with an electrochemical oxygen sensor, is sufficient for the characterisation of the corrosion conditions and the qualitative analysis of the behaviour of the steel constituents. However, the chemical potential/activity significantly changes with temperature, so that, when considering the conditions in a non-isothermal plant, the specification of the oxygen content using a temperature-independent quantity like mole fraction or mass concentration is more favourable. Additionally, oxygen concentrations are more meaningful with respect to the amount of oxygen which is available for the formation of an oxide scale on the steel surface. Translated into requirements for the oxygen control system, this means that the oxygen concentration in the liquid metal must be high enough so that oxides of the steel constituents can form on the steel surface at all temperatures under consideration, but lower than the threshold for the precipitation of oxides of the liquid-metal components in order to prevent plugging of the flow paths in the plant. The relationship between the chemical potential of oxygen and the oxygen concentration in the liquid metal is not only useful for characterising the corrosion conditions, but, together with the respective relationships for the steel constituents, is the basis for the prediction of the behaviour of the steel constituents and numerical simulations of the corrosion processes in oxygen-containing liquid metals.

This report summarises the fundamentals of corrosion and oxygen control in liquid lead (Pb) and lead-bismuth eutectic (LBE), which are promising process media for nuclear applications (coolant, spallation target) and are both examples of a liquid metal that fulfils the pre-requisite for the reduction of steel corrosion by additions of oxygen. Using data on chemical and physical properties provided by the technical literature, mathematical equations are derived, which are helpful for the analysis and

numerical simulation of the behaviour of the primary steel constituents (namely iron (Fe), chromium (Cr) and nickel (Ni)) in oxygen-containing liquid Pb and LBE. Additionally, the measurement of the oxygen potential with electrochemical oxygen sensors and the evaluation of the sensor output are discussed.

# 2 Thermodynamic fundamentals

The thermodynamic criterion for a physical or chemical process to proceed at constant temperature and pressure is that the Gibbs free energy change associated with this process is negative, i.e.,

$$(dG)_{p,T} < 0 \tag{1}$$

For the thermodynamic equilibrium of the process, the free energy G is minimum or

$$(dG)_{p,T} = 0 \tag{2}$$

The free energy is related to the chemical composition of the considered (homogeneous) phases via the partial molar free energy or chemical potential, $\mu_i$, of the involved substances, i, whereby a chemical potential of the substances is assigned to each phase. Mass transfer of substance i between homogenous phases occurs from the phase with the higher $\mu_i$ to that with the lower $\mu_i$. In thermodynamic equilibrium, $\mu_i$ has the same value for all phases involved. In heterogeneous phases, which exhibit local differences in the chemical potentials (composition), mass transfer of substance i analogously occurs along the gradient in $\mu_i$ within the phase. In some cases, the assumption of equilibrium conditions, i.e., the equality of the chemical potentials, at the phase boundaries is justified. In other cases, the composition and therefore the chemical potential is determined by a steady state of mass transfer within the phases and across phase boundaries.

## *2.1 Chemical potential and activity of solutes*

In general, the chemical potential of the substance i in the phase under consideration can be expressed by the chemical potential of i in a standard state, $\mu_i^0$, and a term which depends on the composition of the phase. For a real mixture of gases

$$\mu_i = \mu_i^0 + RT \ln \frac{f_i}{f_i^0} \tag{3}$$

where $f_i$ and $f_i^0$ are the fugacity of i in the gas mixture and the fugacity of i in the chosen standard state, respectively. Considering ideal gases in ideal gas mixtures, the fugacity coincides with the partial pressure of i in the mixture, $p_i$. If the standard state is chosen as the pure gas i at the reference pressure $p^0$ and the temperature under consideration, the chemical potential of an ideal gas in an ideal gas mixture follows as

$$\mu_i = \mu_i^0 + RT \ln \frac{p_i}{p^0} \tag{4}$$

For convenience, the reference pressure is generally chosen as $p^0$ = 1 bar.

In order to have a similar expression for the dependence of the chemical potential on composition for condensed phases (solid, liquid), the activity of the substance i, $a_i$, is introduced, so that

$$\mu_i = \mu_i^0 + RT \ln a_i \tag{5}$$

The relationship between $a_i$ and the concentration of i, $x_i$, in the condensed phase is

$$a_i = \gamma_i x_i \tag{6}$$

where the value of the activity coefficient $\gamma_i$ depends on the chosen reference state, the concentration scale used (mole fraction, mass concentration etc.), temperature and, in general, on the concentration of all components of the considered phase. There are two limiting cases in which $\gamma_i$ is independent of the concentration of the substance i: (1) the ideal solution (Raoult's law; $\gamma_i$ = 1 when $x_i$ is in mole fraction); and (2) the ideal dilute solution (Henry's law). While Raoult's law can often be applied to the solvent of a dilute solution, the relationship between the solute activity and concentration in such a solution often obeys Henry's law. For binary solutions, it follows from the Gibbs-Duhem equation that, if Henry's law is valid for the solute, Raoult's law is valid for the solvent. At reasonably low values of the solute concentration, a small departure of the solute behaviour from Henry's law results in a significantly smaller deviation from Raoult's law for the solvent, so that Raoult's law approximates the solvent behaviour fairly well even if there are deviations of the solute behaviour from Henry's law [1].

In the following, it is assumed that Henry's law applies for the solutes in the dilute solutions considered. In this case, the relationship between the solute activity and concentration is

$$a_i = k_i x_i \tag{7}$$

where the Henry constant of the solute i, $k_i$, is independent of the concentration $x_i$, but depends on temperature and the composition of the solvent (= major components of the solution). In order to determine $k_i$, it is sufficient to know the activity $a_i$ corresponding to one concentration $x_i$ within the range of validity of Henry's law. If Henry's law is valid up to the saturation concentration, $x_{i;s}$, of the solute i,

$$k_i = \frac{1}{x_{i;s}} \tag{8}$$

provided that the reference state for the chemical potential of the solute is appropriately chosen, so that $a_i$ = 1 for the saturated solution. Combining Eqs. (7) and (8) yields

$$a_i = \frac{x_i}{x_{i;s}} \approx \frac{c_i}{c_{i;s}} \tag{9}$$

which means, that in the case regarded, the activity of i at a given temperature simply results from the ratio of the actual concentration and the saturation concentration at this temperature. For the dilute solutions considered, the ratio of concentrations of the solute is practically independent from the chosen concentration scale, so that the solute activity can either be expressed using the mole fraction of the solute ($x_i$ and $x_{i;s}$) or the mass concentration ($c_i$ and $c_{i;s}$), e.g., in mass%.

## *2.2 Dissolution of high-melting metals in a liquid metal*

Regarding the dissolution of a metal M with high melting point, e.g., Fe, Cr or Ni, in a low-melting metal (the liquid metal, e.g., Pb or LBE), an appropriate reference state for the chemical potential of the solute is the pure solid metal M at the temperature under consideration. For this reference state, $a_M = 1$. If no intermetallic compounds are formed between the dissolved and the liquid metal, the saturated solution is in equilibrium with the pure solid solute, so that Eq. (9) can be applied.

As discussed by *Kleppa et al.* [2], the temperature dependence of the saturation concentration of the high-melting metal ($x_{M;s}$ in mole fraction) can be expressed as

$$\ln(x_{M;s}) = \frac{\Delta_{fus}S_M + S_M^E}{R} + \frac{\Delta_{fus}H_M + \Delta_{mix}H_M}{RT} \tag{10}$$

where $\Delta_{fus}S_M$ and $\Delta_{fus}H_M$ are the entropy and enthalpy, respectively, of fusion of the metal M, and $S_M^E$ and $\Delta_{mix}H_M$ are the excess partial molar entropy and the enthalpy of mixing, respectively, for mixing the molten metal M with the solvent (the liquid metal). R and T are the universal gas constant and thermodynamic temperature, respectively. For low saturation concentrations of the metal M (e.g., below ~ 2 at% for the dissolution of copper (Cu) in liquid Pb [2]), i.e., for a limited range of temperatures, the sum of entropies ($\Delta_{fus}S_M$ = const., $S_M^E = 0$) and enthalpies can be regarded as independent of temperature, so that the first term on the right hand side of Eq. (10) and the temperature coefficient are constant. Accordingly, experimentally determined saturation concentrations (solubility) which fall into this limited temperature range are presented using an equation of the type

$$\log(c_{M;s}/\,\text{mass\%}) = A + \frac{B}{T/\,K} \tag{11}$$

with constants A and B and temperature, T, in K.

## *2.3 Dissolution of oxygen in liquid metals*

As oxygen is a diatomic gas at the temperatures under consideration, the natural reference state for the chemical potential of oxygen is the pure gas ($O_2$) at 1 bar. The equivalent of the activity in a condensed phase is the ratio of the oxygen partial pressure and the reference pressure (ideal gas phase). Assuming, that oxygen dissolves atomically (or ionically) in a liquid metal, i.e., according to the reaction equation

$$\frac{1}{2}O_2(g) \rightleftarrows [O]_{\text{liquid metal}} \tag{12}$$

with equilibrium constant

$$K_{O_2/[O]} = \frac{a_O}{\sqrt{p_{O_2}/p^0}} \tag{13}$$

and assuming furthermore, that the dissolved oxygen obeys Henry's law (Eq. 7) with Henry constant $k_O$, the oxygen concentration, $x_O$, in the liquid metal is proportional to the square root of the oxygen partial pressure above the solution,

$$x_O = \frac{K_{O_2/[O]}}{k_O}\sqrt{p_{O_2}/p^0} \tag{14}$$

(Sievert's law [3]). If Henry's law and, therefore, Sievert's law is valid up to the saturation concentration of oxygen, $x_{O;s}$, with corresponding equilibrium partial pressure above the solution, $p_{O_2;s}$, it follows that

$$\sqrt{\frac{p_{O_2}}{p_{O_2;s}}} = \frac{x_O}{x_{O;s}} \approx \frac{c_O}{c_{O;s}} \tag{15}$$

Eq. (15) is the equivalent of Eq. (9) for the atomic or ionic dissolution of a diatomic gas. The temperature dependence of the oxygen saturation concentration (solubility) in liquid metals generally follows an equation of the type of Eq. (11).

Oxygen saturation of a liquid metal is characterised by the precipitation of solid or liquid oxides, with the most stable oxide of the least noble component(s) of the liquid metal (in general a mixture of diverse metals) precipitating first from the oxygen-saturated solution. Hence, the oxygen partial pressures in Eq. (15) can be substituted by the activity of this oxide, which will be demonstrated for an oxide of general type $M_yO_z$. The formation of $M_yO_z$ follows the stoichiometric equation

$$\frac{y}{z}[M]_{\text{liquid metal}} + \frac{1}{2}O_2(g) \rightleftarrows \frac{1}{z}[M_yO_z]_{\text{liquid metal}} \tag{16}$$

where it is assumed that the liquid metal is not saturated with oxygen, so that the oxide does not form a phase of its own, but is dissolved in the liquid metal. Taking pure $M_yO_z$ in the stable state of aggregation (solid or liquid) as the reference state for the chemical potential of the oxide, the actitvity of $M_yO_z$, $a_{M_yO_z}$, is <1. The relation between the oxygen partial pressure above the solution, $p_{O_2}$, and the oxide activity follows from the equilibrium constant corresponding to Eq. (16), $K_{M/M_yO_z}$, as

$$\sqrt{\frac{p_{O_2}}{p^0}} = \frac{K_{M/M_yO_z}}{a_M^{y/z}}a_{M_yO_z}^{1/z} \tag{17}$$

The activity of the metallic component(s) of the oxide, $a_M$, is constant and $a_{M_yO_z} = 1$ for the saturated solution, so that substituting $p_{O_2}$ and $p_{O_2;s}$ in Eq. (15) yields

$$a_{M_yO_z}^{1/z} = \frac{x_O}{x_{O;s}} \approx \frac{c_O}{c_{O;s}} \tag{18}$$

For essentially pure liquid Pb and LBE without significant amounts of impurities, the oxide that precipitates first from the oxygen-saturated solution is lead monoxide, PbO, for which z = 1 in Eq. (18). Thus,

$$a_{PbO} = \frac{x_O}{x_{O;s}} \approx \frac{c_O}{c_{O;s}} \tag{19}$$

Eq. (19) is very similar to Eq. (9), so that some authors dealing with the dissolution of oxygen in Pb or LBE equate the ratio of the actual oxygen concentration and the oxygen saturation concentration with the oxygen activity (or oxygen thermodynamic activity, OTA) $a_O$. However, it should be noted that for thermodynamic calculations on the basis of this activity the standard chemical potential of PbO must be used and not the standard potential for atomic oxygen (which in fact cannot easily be calculated). Additionally, chemical reactions of oxygen in the liquid metal have to be formulated for the conversion of dissolved PbO. In order to emphasise these facts, the expression $a_{PbO}$ is preferred in this report.

## *2.4 Stability of oxides*

The stability of oxides is of major importance for the performance of steels in oxygen-containing liquid metals. For steel constituents which exhibit a significant solubility in the liquid metal, the formation of a dense oxide scale on the steel surface may considerably reduce the dissolution rate or completely prevent dissolution, as the respective steel constituents have to diffuse through the oxide scale before they can be dissolved by the liquid metal at the scale surface. Additionally, the precipitation of oxides lowers the equilibrium solubility of the steel constituents participating in the oxidation processes according to the solubility product of the oxides. Besides the main steel constituents (Fe, Cr, Ni), minor components like aluminium (Al) and silicon (Si) which form very stable oxides must also be considered. With respect to the estimation of the optimum range for the enrichment of oxygen in the liquid metal and the determination of the oxygen partial pressure above the saturated solution (which is used in Eq. (15)), the stability of the oxides of the liquid-metal components is of importance.

The formation of a solid oxide of general type $M_yO_z$ from the solid or liquid metal M and 1 mol gaseous oxygen ($O_2$) can be described by the stoichiometric equation

$$\frac{2y}{z} M(s,l) + O_2(g) \rightleftarrows \frac{2}{z} M_yO_z(s) \tag{20}$$

with equilibrium constant

$$K_{M/M_yO_z} = \frac{a_{M_yO_z}^{2/z}}{a_M^{2y/z}(p_{O_2}/p^0)} \tag{21}$$

In Eq. (21), $a_M$ is the activity of the oxidised metal, $a_{M_yO_z}$ is the activity of the oxide and $p_{O_2}$ is the oxygen partial pressure which depends on the oxygen concentration in the liquid metal according to Eq. (15). $p^0$ is the reference pressure of the chemical potential of gaseous oxygen ($p^0$ = 1 bar). The change of the Gibbs free energy for the conversion of 1 mol $O_2$, $\Delta G$, results from the standard free energy of formation of the oxide, $\Delta_f G^0_{M/M_yO_z}$, and the equilibrium constant as

$$\Delta G = \Delta_f G^0_{M/M_yO_z} + RT \ln K_{M/M_yO_z} \tag{22}$$

where $\Delta_f G^0_{M/M_yO_z}$ can be calculated from the chemical potentials of the participating substances in their standard state or measured by appropriate techniques. The temperature dependence of $\Delta_f G^0_{M/M_yO_z}$ has the general form

$$\Delta_f G^0_{M/M_yO_z}/(\mathrm{kJ\,mol^{-1}}) = C + D\,(T/K) \tag{23}$$

with constants C and D and temperature, T, in K.

According to the thermodynamic criteria for the progress of a chemical process (Eq. 1) and the establishment of chemical equilibrium (Eq. 2), it follows from Eq. (22) that oxidation of metal M occurs, if

$$RT \ln\left(\frac{a_M^{2y/z}(p_{O_2}/p^0)}{a_{M_yO_z}^{2/z}}\right) \geq \Delta_f G^0_{M/M_yO_z} \tag{24}$$

Regarding the formation of pure oxide ($a_{M_yO_z}$ = 1) from the pure metal ($a_M$ = 1), the threshold oxygen partial pressure (or dissociation pressure of the oxide) for the formation of $M_yO_z$ follows as

$$p_{O_2}^{M/M_yO_z}/\mathrm{bar} = \exp\frac{\Delta_f G^0_{M/M_yO_z}}{RT} \tag{25}$$

However, it should be noted that in the case of alloys (steels, LBE) the oxygen partial pressure necessary for the formation of a specific (pure) oxide is somewhat higher than according to Eq. (24), as $a_M$ < 1. Values for the constants C and D in Eq. (23) for oxides which are relevant for the oxidation of steels and oxygen-containing Pb and LBE are summarised in Table 1. The resulting $\Delta_f G^0_{M/M_yO_z}$ is plotted as a function of temperature in Fig. 1. In the case of the ternary oxides containing two metallic components, it was assumed that the oxide of the less-noble metal forms first.

***Table 1 –*** *Thermodynamic data and temperature range of validity for the formation of oxides of selected steel constituents and liquid Pb and Bi*

| | $\Delta_f G^0_{M/M_yO_z}/(\text{kJ mol}^{-1}) = C + D\,(T/K)$ | | Source |
|---|---|---|---|
| | C | D | |
| $\frac{4}{3}Bi_{(l)} + O_{2(g)} \rightleftarrows \frac{2}{3}\alpha\text{–}Bi_2O_{3(s)}$ | – 388.9 (299 ≤ T/°C ≤ 715) | 0.1959 | [4] |
| $2Pb_{(l)} + O_{2(g)} \rightleftarrows 2\beta - PbO_{(s)}$ | – 437.96 (339 ≤ T/°C ≤ 838) | 0.19926 | [5] |
| $2Ni_{(s)} + O_{2(g)} \rightleftarrows 2NiO_{(s)}$ | – 473.75 | 0.1767 | |
| $2Ni_{(s)} + 2Cr_2O_{3(s)} + O_{2(g)} \rightleftarrows 2NiCr_2O_{4(s)}$ | – 492.26 | 0.1868 | |
| $2Ni_{(s)} + 2\alpha\text{–}Al_2O_{3(s)} + O_{2(g)} \rightleftarrows 2NiAl_2O_{4(s)}$ | – 486.53 | 0.1580 | |
| $2Fe_{(s)} + O_{2(g)} \rightleftarrows 2FeO_{(s)}$ | – 529.77(†) | 0.1302 | |
| $\frac{3}{2}Fe_{(s)} + O_{2(g)} \rightleftarrows \frac{1}{2}Fe_3O_{4(s)}$ | – 549.58 | 0.1537 | |
| $6FeO_{(s)} + O_{2(g)} \rightleftarrows 2Fe_3O_{4(s)}$ | – 608.94(‡) | 0.2241 | |
| $2Fe_{(s)} + 2\alpha\text{–}Al_2O_{3(s)} + O_{2(g)} \rightleftarrows 2FeAl_2O_{4(s)}$ | – 640.28 | 0.1495 | (∗) |
| $2Fe_{(s)} + 2Cr_2O_{3(s)} + O_{2(g)} \rightleftarrows 2FeCr_2O_{4(s)}$ | – 651.27 | 0.1495 | |
| $\frac{4}{3}Cr_{(s)} + O_{2(g)} \rightleftarrows \frac{2}{3}Cr_2O_{3(s)}$ | – 751.22 | 0.1700 | |
| $Si_{(s)} + O_{2(g)} \rightleftarrows SiO_{2(s)}$ | – 908.28 | 0.1782 | |
| $\frac{4}{3}Al_{(s)} + O_{2(g)} \rightleftarrows \frac{2}{3}\alpha\text{–}Al_2O_{3(s)}$ | – 1118 (200 ≤ T/°C ≤ 800) | 0.2096 | |

(∗): Interpolation of thermodynamic data provided by the database of the software HSC [6]

(†): Value has been corrected by –1.46 kJ/mol to account for FeO being stable at T ≥ 570°C

(‡): Value has been corrected by 4.43 kJ/mol to account for FeO being stable at T ≥ 570°C

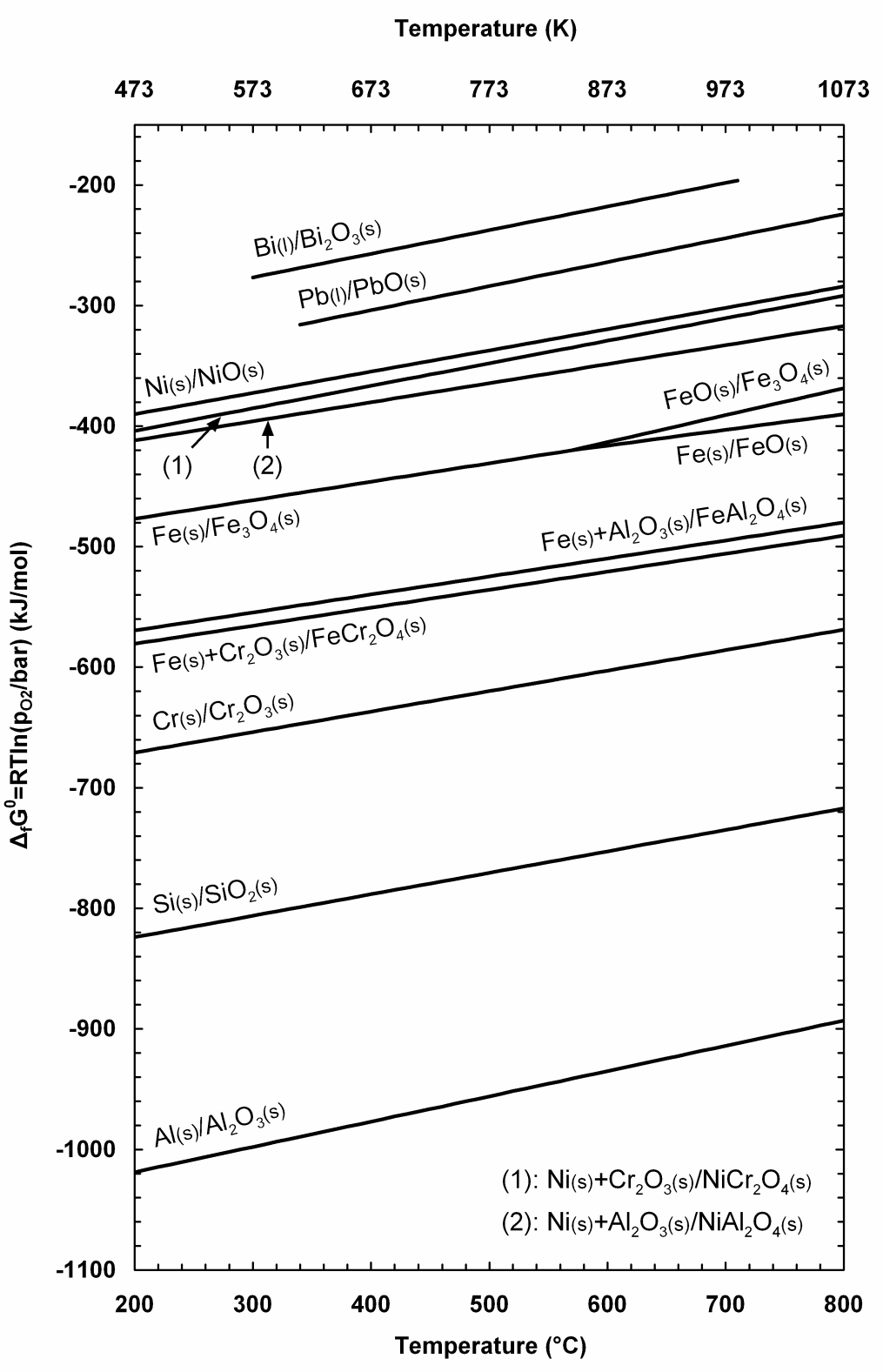


***Figure 1 –*** *Standard Gibbs free energy of formation, $\Delta_f G^0$, as a function of temperature for various oxides which are relevant for the oxidation of steels and oxygen-containing Pb and LBE. See Table 1 for details on the thermodynamic data used for the construction of the diagram.*

## *2.5 Solubility product of oxides*

Eq. (21) implies that, if the oxide $M_yO_z$ is stable and forms a separate pure phase ($a_{M_yO_z} = 1$), the product of the metal activity, $a_M$, and the oxygen activity, $a_O$, in the liquid metal to the power of the respective number of moles in 1 mol oxide (y and z, respectively) is constant, i.e.,

$$a_M^y \, a_O^z = K_S^{M_yO_z} \tag{26}$$

where $p_{O_2}$ in Eq. (21) has been substituted by $a_O$ using Eq. (12). $K_S^{M_yO_z}$ is the temperature-dependent solubility product of the oxide $M_yO_z$ in the regarded liquid metal. Substituting the activities in Eq. (26) by the concentrations $x_M$ and $x_O$ yields

$$x_M^y \, x_O^z = K_{S(x)}^{M_yO_z} \tag{27}$$

where $K_{S(x)}^{M_yO_z}$ is the solubility product for the chosen concentration scale. According to Eq. (27), the concentration of dissolved metal M increases with decreasing oxygen content and is maximum for the oxygen concentration corresponding to the dissociation partial pressure of the oxide, $p_{O_2}^{M/M_yO_z}$. This maximum concentration of dissolved M coincides with the saturation concentration $x_{M;s}$ in the absence of dissolved oxygen. At even lower oxygen concentration, the pure metal and not the oxide precipitates first from the solution. Analogously, the concentration of dissolved oxygen increases with decreasing concentration of dissolved metal M, with the upper limit being the oxygen saturation concentration $x_{O;s}$ in the absence of metallic solutes. In this case, the activity of dissolved metal M is so low that oxides of the constituents of the solvent (liquid metal/alloy) precipitate first. Accordingly, the solubility product of metal oxides has to be regarded when predicting the amount of metals dissolved at a given temperature in the presence of oxygen and the precipitation of metals and oxygen in the form of oxides as a function of temperature.

The starting point for the calculation of $K_{S(x)}^{M_yO_z}$ from thermodynamic data is the substitution of $x_M$ and $x_O$ on the left hand side of Eq. (27). If Henry's law holds for the dissolved metal M up to the saturation concentration in the absence of oxygen, $x_{M;s}$, and Sievert's law is valid for dissolved oxygen up to the saturation concentration in the absence of metallic solutes, $x_{O;s}$, it follows from Eq. (9) and Eq. (15) that

$$x_M^y \, x_O^z = x_{M;s}^y \, x_{O;s}^z \, \frac{a_M^y (p_{O_2}/p^0)^{z/2}}{(p_{O_2;s}/p^0)^{z/2}} \tag{28}$$

where $p_{O_2}$ is the oxygen partial pressure for the equilibrium between the metallic solute M, oxygen and pure solid $M_yO_z$ ($a_{M_yO_z} = 1$). Taking into account, that the equilibrium constant $K_{M/M_yO_z}$ in Eq. (21) can be substituted by the standard Gibbs free energy of formation of $M_yO_z$, $\Delta_f G^0_{M/M_yO_z}$, using Eq. (22) with $\Delta G = 0$ (equilibrium conditions), $p_{O_2}$ is given by

$$\frac{p_{O_2}}{p^0} = \frac{1}{a_M^{2y/z}} \exp \frac{\Delta_f G^0_{M/M_yO_z}}{RT} \tag{29}$$

$p_{O_2;s}$ on the right hand side of Eq. (28) is the partial pressure above the oxygen saturated solution in the absence of metallic solutes and is determined by the equilibrium between the liquid metal, oxygen and the oxide, the precipitation of which limits the oxygen solubility in the absence of metallic solutes. Considering only those liquid metals for which PbO precipitates first from the oxygen saturated solution (liquid Pb, LBE), it follows by analogy that

$$\frac{p_{O_2;s}}{p^0} = \frac{1}{a_{Pb}^2} \exp \frac{\Delta_f G^0_{Pb/PbO}}{RT} \tag{30}$$

(y = 1 and z = 1 in Eq. (29) for the formation of PbO). Inserting Eq. (29) and Eq. (30) on the right hand side of Eq. (28) and comparing with Eq. (27) yields

$$K^{M_yO_z}_{S(x)} = x^y_{M;s}\, x^z_{O;s}\, a^z_{Pb} \exp\left\{\frac{z}{2RT}(\Delta_f G^0_{M/M_yO_z} - \Delta_f G^0_{Pb/PbO})\right\} \tag{31}$$

or

$$\log K^{M_yO_z}_{S(x)} = y \log x_{M;s} + z\left\{\log x_{O;s} + \log a_{Pb} + \frac{\log e}{2RT}(\Delta_f G^0_{M/M_yO_z} - \Delta_f G^0_{Pb/PbO})\right\} \tag{32}$$

The saturation concentrations on the right hand side of Eq. (31) and Eq. (32) account for the dependence of the value of $K^{M_yO_z}_{S(x)}$ on the chosen concentration scale (mole fraction, mass concentration in mass% etc.).

# 3 Lead

## *3.1 Dissolution of oxygen*

The dissolution and especially the solubility limit of oxygen in liquid Pb has been investigated in numerous studies. Most of the results published before 1997 were summarised and analysed by *Risold et al.* [7], who noticed a large spread in the solubility data reflecting the experimental difficulties in the various techniques applied for the solubility measurements. However, at intermediate temperatures between about 500° and 886°C (886°C is the temperature at which a PbO-rich liquid begins to form), the correspondence between the results obtained from different experimental methods is comparatively good, so that the solubility data for this temperature range can be regarded as reliable. Recently, the oxygen solubility in the temperature range from 542°-817°C was measured by *Ganesan et al.* [8] using an electrochemical method, with the results showing good correspondence with other investigations performed at higher and slightly lower temperatures using the same type of technique. The temperature dependence of the saturation concentration of oxygen, $c_{O;s}$, determined by *Ganesan et al.* is

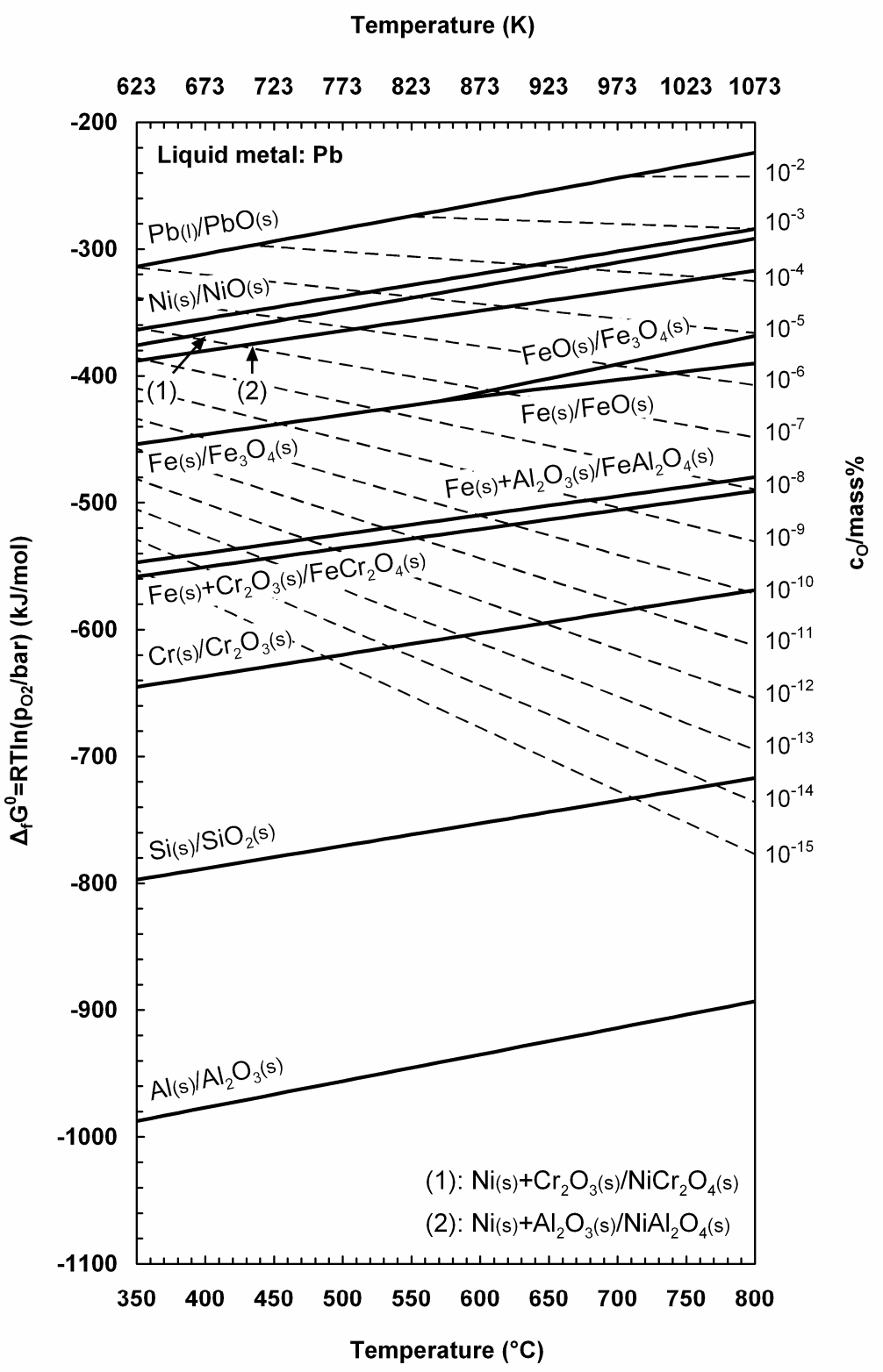


***Figure 2 –*** *Dependence of the thermodynamic stability of selected oxides of steel constituents on temperature and the concentration of oxygen dissolved in liquid Pb.*

$$\log(c_{O;s}/\text{mass\%}) = 3.21 - \frac{5100}{T/K} \quad (33)$$

It is assumed that Eq. (33) approximates $c_{O;s}$ also for lower temperatures.

Measurements of the activity coefficient of oxygen in liquid Pb defined by Eq. (6) show, that, at temperatures above 750°C, the activity coefficient slightly decreases with increasing oxygen concentration. With decreasing temperature, the dependence of the activity coefficient on the oxygen concentration becomes less pronounced [7]. In the temperature range from 510° to 700°C, the activity coefficient is apparently independent from the oxygen concentration [9], so that Henry's law (Eq. (7)) and, therefore, also Sievert's law (Eq. (14)) can be applied to the dissolution of oxygen in liquid Pb. In this case, the dependence of the oxygen partial pressure above the liquid metal, $p_{O_2}$, on the concentration of dissolved oxygen, $c_O$, and temperature, T, follows from Eq. (15) as

$$p_{O_2}/\text{bar} = (c_O/\text{mass\%})^2 \exp\left\{9.1827 - \frac{29188}{T/K}\right\} \quad (34)$$

where the oxygen partial pressure above the saturated solution, $p_{O_2;s}$, was substituted using Eq. (30) (with $a_{Pb}$ = 1) and thermodynamic data for the Pb/PbO equilibrium from Table 1. $c_{O;s}$ was substituted using Eq. (33). Amongst others, Eq. (34) can be used to supplement Fig. 1 with lines of constant oxygen concentration in order to illustrate the dependence of the stability of oxides on temperature and the concentration of oxygen dissolved in the liquid metal (Fig. 2). The lines of constant $c_O$ are especially helpful for analysing the oxide stability along the flow path in non-isothermal plants.

The activity of PbO, $a_{PbO}$, in unsaturated liquid Pb as a function of the oxygen concentration and temperature results form inserting Eq. (33) into Eq. (19), i.e.,

$$a_{PbO} = (c_O/\text{mass\%}) \exp\left\{-7.3913 + \frac{11743}{T/K}\right\} \quad (35)$$

## *3.2 Dissolution of metals and solubility products*

In this section, experimental data on the solubility of the main steel constituents, namely Fe, Cr and Ni, in liquid Pb are presented and discussed. Furthermore, the solubility product of the corresponding metal oxides is calculated using Eq. (31) (with $a_{Pb}$ = 1) and thermodynamic data for the metal/metal oxide equilibria from Table 1. It is assumed that the temperature-dependent saturation concentration of oxygen, $c_{O;s}$, obeys Eq. (33) over the whole temperature range considered (350°-800°C).

### *3.2.1 Iron*

Because the dissolution of Fe in liquid Pb is important for the behaviour of steels in contact with the liquid metal, the saturation concentration of Fe, $c_{Fe;s}$, was measured by several authors. However, the published experimental data is contradictory with respect to the best type of equation to reproduce the temperature de-

pendence of $c_{Fe;s}$ and the significance of the $\alpha$-$\gamma$ transition for the solubility of Fe in liquid BP. The $\alpha$-$\gamma$ transition (at 910°C) occurs outside the temperature range of interest for the application of liquid Pb as a process medium, but a negligible influence would mean that experimental data for > 910°C can be used to confirm the temperature dependence of the solubility at lower temperatures and indicate that there is no general difference between the dissolution of Fe from ferritic and austenitic steels. Only the different Fe activity in these steels has to be considered.

Measurements of the saturation concentration of Fe in liquid BP, the results of which correspond comparatively well with each other, are those performed by *Weeks et al.* [10] and *Stevenson et al.* [11]. *Weeks et al.* investigated the temperature range from 400° to 850°C and found that their experimental data is reproduced best by the equation

$$\log(c_{Fe;s}/\text{mass\%}) = 5.051 - \frac{11728}{T/K} + \frac{3.633 \times 10^6}{(T/K)^2} \qquad (36)$$

Eq. (36) implies, that the saturated solutions of Fe in liquid Pb do not obey Henry's law over the entire temperature range from 400° to 850°C, although the saturation concentrations are merely in the order of $10^{-3}$ to $10^{-2}$ at.%. However, the single data points scatter remarkably around the curve resulting from Eq. (36), which is especially true for < 600°C. Also the linear $\log c_{Fe;s}$-1/T curve (assumption that Henry's law applies) suggested by *Weeks et al.* for the lower end of the investigated temperature range deviates significantly from the experimental data, the more so, the lower the temperature [10].

For temperatures between 600° and 750°C, *Weeks et al.* approximated the temperature dependence of the saturation concentration of Fe in liquid Pb using the equation

$$\log(c_{Fe;s}/\text{mass\%}) = 1.824 - \frac{4860}{T/K} \qquad (37)$$

This linear relation between $\log c_{Fe;s}$ and 1/T (dashed line in Fig. 3) is in accordance with the results of Eq. (36) for this temperature range and also coincides well with the Fe solubility at temperatures between about 750° and 1300°C measured by *Stevenson et al.* [11] (solid line and open diamonds, respectively, in Fig. 3). Therefore, it is assumed that Eq. (37) describes the saturation concentration of Fe in the temperature range from 600° to 1300°C, which implies that the influence of the $\alpha$-$\gamma$ transition on the dissolution of Fe in liquid Pb is negligible and that Henry's law is valid for the saturated solutions at high temperatures. But, if Henry's law is valid at high temperatures, it should also be applicable at low temperatures, so that Eq. (37) can presumably also be used to calculate $c_{Fe;s}$ for temperatures below 600°C. The discrepancy between the experimental data of *Weeks et al.* and this equation for lower temperatures may be explained by experimental errors. However, only a re-determination of the Fe solubility at < 600°C can confirm or disprove the validity of Eq. (37) in this temperature range.

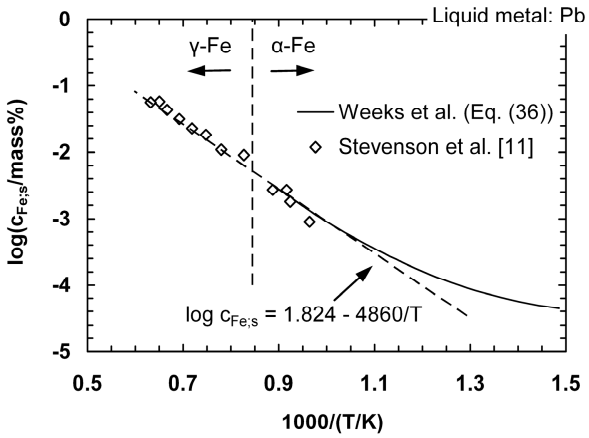


***Figure 3 –*** *Temperature dependence of the saturation concentration of Fe in liquid Pb according to measurements by Weeks et al. and Stevenson et al.*

Using Eq. (37) for the saturation concentration $c_{Fe;s}$, the solubility products of magnetite, $Fe_3O_4$, and wuestite, FeO, in liquid Pb result as

**$Fe_3O_4$:**
$$(c_{Fe}/\text{mass\%})^3 (c_O/\text{mass\%})^4 = \exp\left\{31.206 - \frac{107309}{T/\text{K}}\right\} \tag{38}$$

**FeO:**
$$(c_{Fe}/\text{mass\%})(c_O/\text{mass\%}) = \exp\left\{7.4382 - \frac{28455}{T/\text{K}}\right\} \tag{39}$$

These equations were used to calculate the maximum concentration of dissolved Fe as a function of the oxygen concentration in the region of stability of the respective oxide with temperature as a variable parameter (Fig. 4). The boundary lines between the regions of stability follow from the condition that the concentration of dissolved Fe has to be the same for the phases on both sides of the boundary (e.g., Fe/$Fe_3O_4$; FeO/$Fe_3O_4$). The concentration of dissolved oxygen is restricted by the precipitation of PbO which occurs at the oxygen saturation concentration in the absence of dissolved metals, $c_{O;s}$, given by Eq. (33). In the region of stability of PbO, the maximum concentration of dissolved metals depends only on temperature and, in the case of Fe, follows from the solubility product of $Fe_3O_4$ with $c_O = c_{O;s}$. At low oxygen concentrations, the up-take of Fe by the liquid metal is determined by the saturation concentration in the absence of Fe oxides, $c_{Fe;s}$. The diagram in Fig. 4 is especially useful for the characterisation of the corrosion conditions for Fe and steels in liquid Pb at a given temperature and oxygen concentration. As a first approximation for the analysis of non-isothermal corrosion processes, the oxide stability and changes in the concentration of dissolved Fe along lines of constant oxygen concentration can be regarded, but it should be kept in mind, that the oxygen concentration may change as a consequence of oxide formation or dissolution.

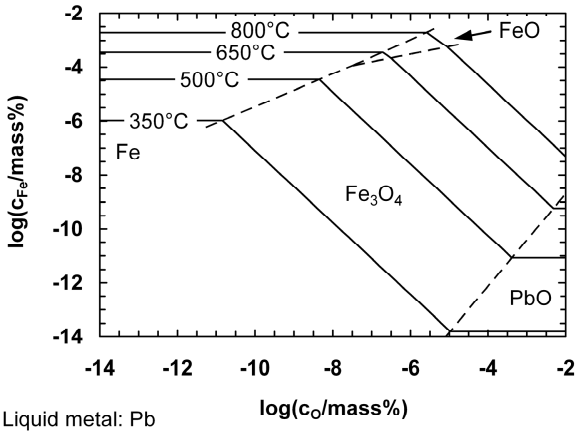


***Figure 4 –*** *Maximum concentration of Fe dissolved in liquid Pb in the presence of dissolved oxygen (solid lines with temperature as variable parameter). The dashed lines define the regions of thermodynamic stability of Fe, Fe oxides and PbO.*

### *3.2.2 Chromium and nickel*

The dissolution of Cr and Ni in liquid Pb were both investigated by *Alden et al.* [12]. In the case of Cr, the experimental data on the saturation concentration $c_{Cr;s}$ covers the temperature range from 900° to 1200°C and can be reproduced by the equation

$$\log(c_{Cr;s}/\,\mathrm{mass\%}) = 3.88 - \frac{6949}{T/\,\mathrm{K}} \tag{40}$$

The solubility of Cr is comparatively low (0.6 at.% at 1200°C), so that the saturated solutions presumably obey Henry's law and Eq. (40) can be used to extrapolate $c_{Cr;s}$ to lower temperatures.

The solubility of Ni in liquid Pb, which was measured at temperatures between about 370° and 1240°C, is considerably higher (19 at.% at 1200°C) and, therefore, the saturated solutions do not obey Henry's law over the entire temperature range investigated. For temperatures up to about 800°C, the saturation concentration of Ni in liquid Pb, $c_{Ni;s}$, can be approximated by

$$\log(c_{Ni;s}/\,\mathrm{mass\%}) = 1.30 - \frac{1381}{T/\,\mathrm{K}} \tag{41}$$

Using Eq. (40) and Eq. (41) for $c_{Cr;s}$ and $c_{Ni;s}$, respectively, the solubility products of chromia, $Cr_2O_3$, and nickel monoxide, NiO, were calculated, i.e.,

**$Cr_2O_3$:**
$$(c_{Cr}/\,\mathrm{mass\%})^2(c_O/\,\mathrm{mass\%})^3 = \exp\left\{34.763 - \frac{123745}{T/\,\mathrm{K}}\right\} \tag{42}$$

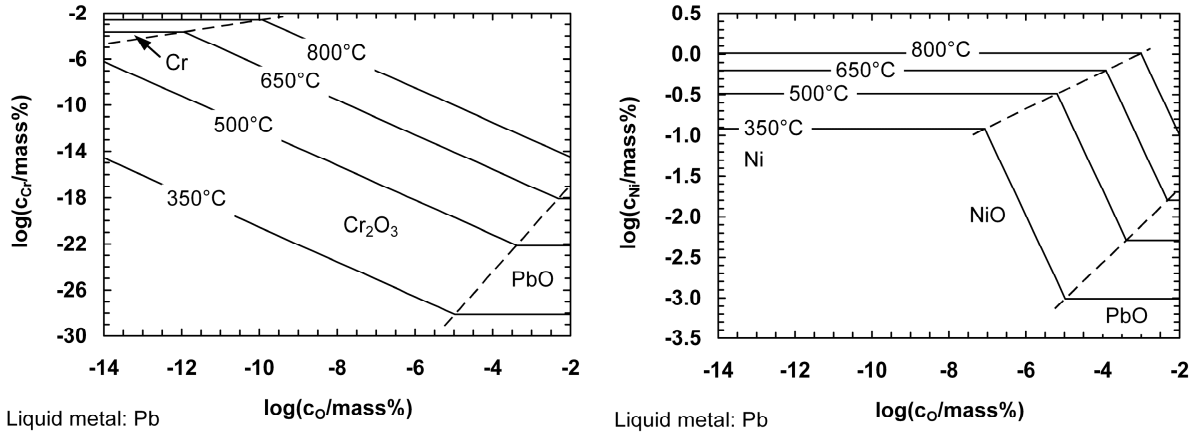


***Figure 5 –*** *Maximum concentration of dissolved Cr (left) and Ni (right) in oxygen-containing liquid Pb for temperatures between 350° and 800°C.*

**NiO:**
$$(c_{Ni}/\text{mass\%})(c_O/\text{mass\%}) = \exp\left\{9.0280 - \frac{17075}{T/K}\right\} \tag{43}$$

According to Eq. (42), the maximum concentration of dissolved Cr in oxygen-containing liquid Pb is very low (Fig. 5, left), as a consequence of the high stability of $Cr_2O_3$. The decrease of the maximum concentration of dissolved Ni due to the formation of NiO sets in at comparatively high oxygen concentrations and is considerably less pronounced (Fig. 5, right). Of the main constituents of steels, Ni exhibits by far the highest solubility in liquid Pb.

# 4 Lead-bismuth eutectic

## *4.1 Activity of lead and bismuth in liquid lead-bismuth alloys*

The thermodynamics of liquid Pb-Bi alloys was the subject of several investigations which were reviewed by *Hultgren et al.* [13], and more recently by *Gokcen* [14] and *Yoon et al.* [15]. Based on published experimental results, *Gokcen* derived equations for the excess partial molar free energies of Pb and Bi, $G^E_{Pb}$ and $G^E_{Bi}$, as a function of the thermodynamic temperature in degrees Kelvin (K) and the composition of the binary alloy (mole fractions $x_{Pb}$ and $x_{Bi}$, where $x_{Pb} + x_{Bi} = 1$). These equations are

$$\begin{aligned} G^E_{Pb}/(\text{J mol}^{-1}) &= (650 - 2.863\,T/K)\,x^2_{Bi} - \\ &- (16200 - 5.994\,T/K)\,x^3_{Bi} + (12150 - 4.215\,T/K)\,x^4_{Bi} \end{aligned} \tag{45}$$

and

$$\begin{aligned} G^E_{Bi}/(\text{J mol}^{-1}) &= (650 - 2.302\,T/K)\,x^2_{Pb} - \\ &- (16200 - 5.264\,T/K)\,x^3_{Pb} + (12150 - 4.215\,T/K)\,x^4_{Pb} \end{aligned} \tag{46}$$

From the thermodynamic parameters presented by *Yoon et al*., it follows that

$$G_{Pb}^{E}/(J\,mol^{-1}) = -(4807.37 + 1.25\,T/K)\,x_{Bi}^{2} \tag{47}$$

and

$$G_{Bi}^{E}/(J\,mol^{-1}) = -(4807.37 + 1.25\,T/K)\,x_{Pb}^{2} \tag{48}$$

The excess partial molar free energy of substance i, $G_i^E$, is related to the activity coefficient $\gamma_i$ in Eq. (6) according to

$$\gamma_i = \exp\left\{\frac{G_i^E}{RT}\right\} \tag{49}$$

As a basis for judging the accuracy of the two sets of equations, the results of calculations are compared with experimental data, using data which was available to

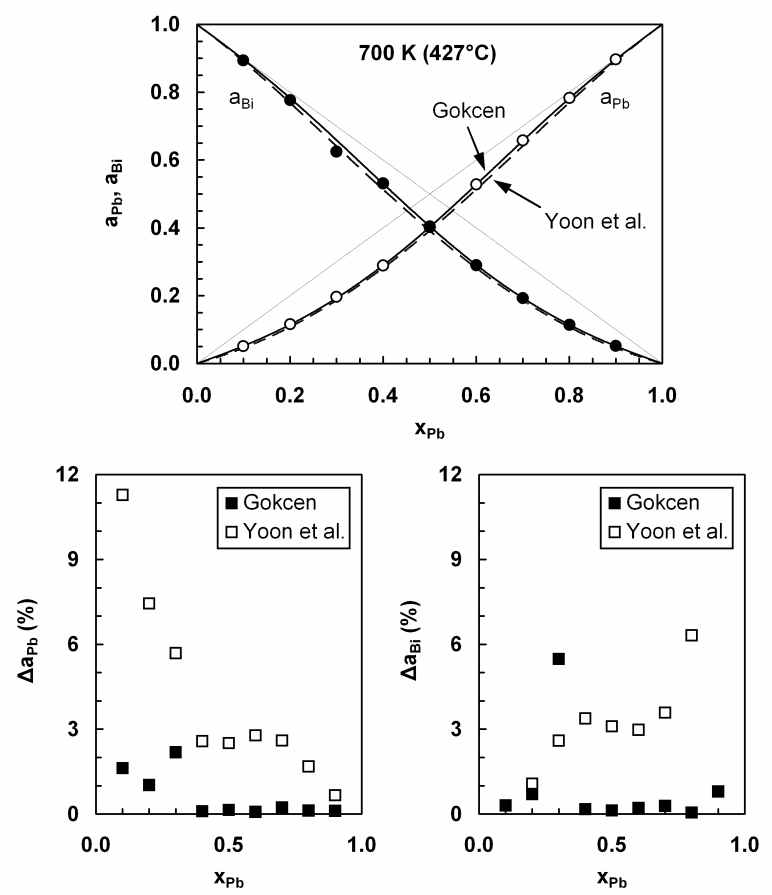


***Figure 6 –*** *Thermodynamic activities of Pb and Bi in liquid Pb-Bi alloys at 427°C calculated from the excess partial molar free energies of Pb and Bi according to Gokcen and Yoon et al., respectively, in comparison to experimental data from Roy et al. (open and solid circles). Bottom: Relative deviation of the calculated thermodynamic activities from the experimental data for Pb (left) and Bi (right).*

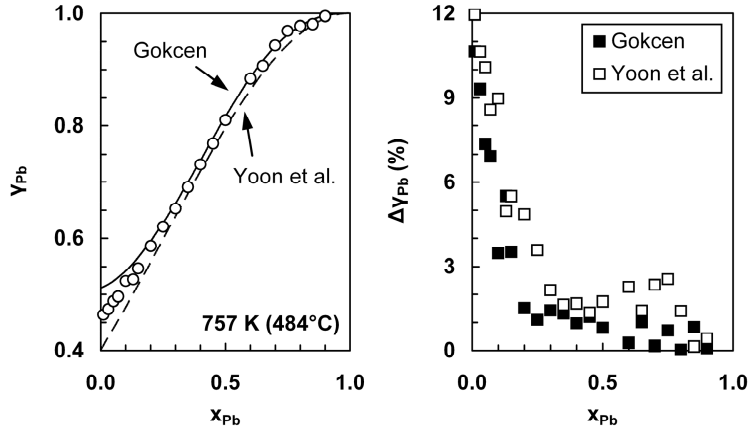


***Figure 7 –*** *Activity coefficient of Pb, $\gamma_{Pb}$, in liquid Pb-Bi alloys at 484°C calculated from the excess partial molar free energies of Pb and Bi according to Gokcen and Yoon et al., respectively, in comparison to experimental data from Moser (open circles). Right: Relative deviation of calculated activity coefficients from the experimental data.*

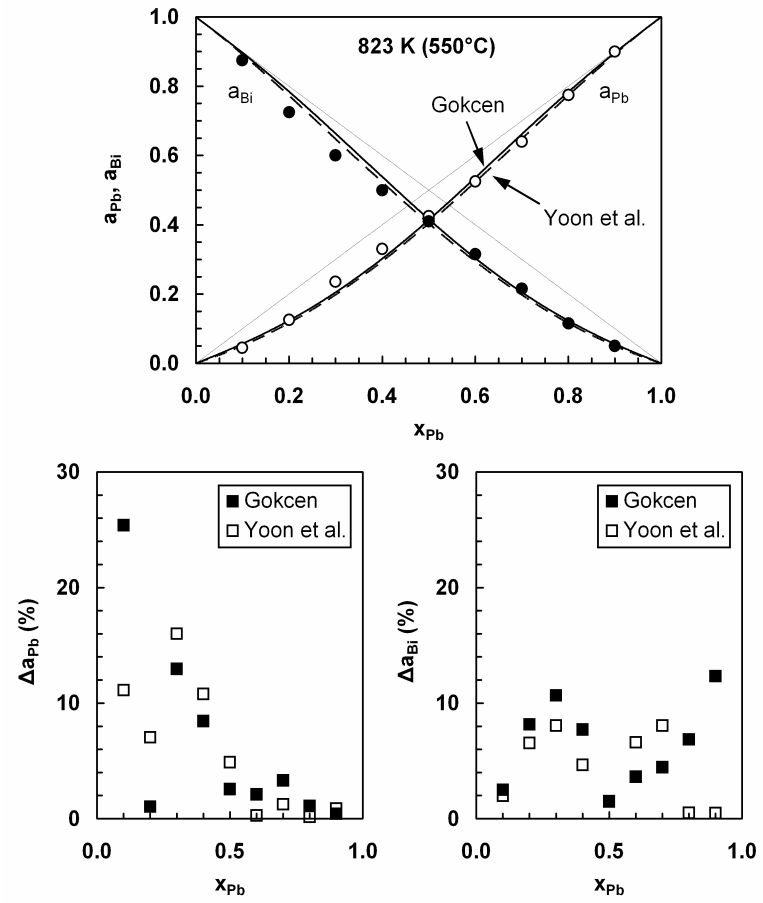


***Figure 8 –*** *Thermodynamic activities of Pb and Bi in liquid Pb-Bi alloys at 550°C calculated from the excess partial molar free energies of Pb and Bi according to Gokcen and Yoon et al., respectively, in comparison to experimental data from Agarwala et al. (open and solid circles). Bottom: Relative deviation of the calculated thermodynamic activities from the experimental data for Pb (left) and Bi (right).*

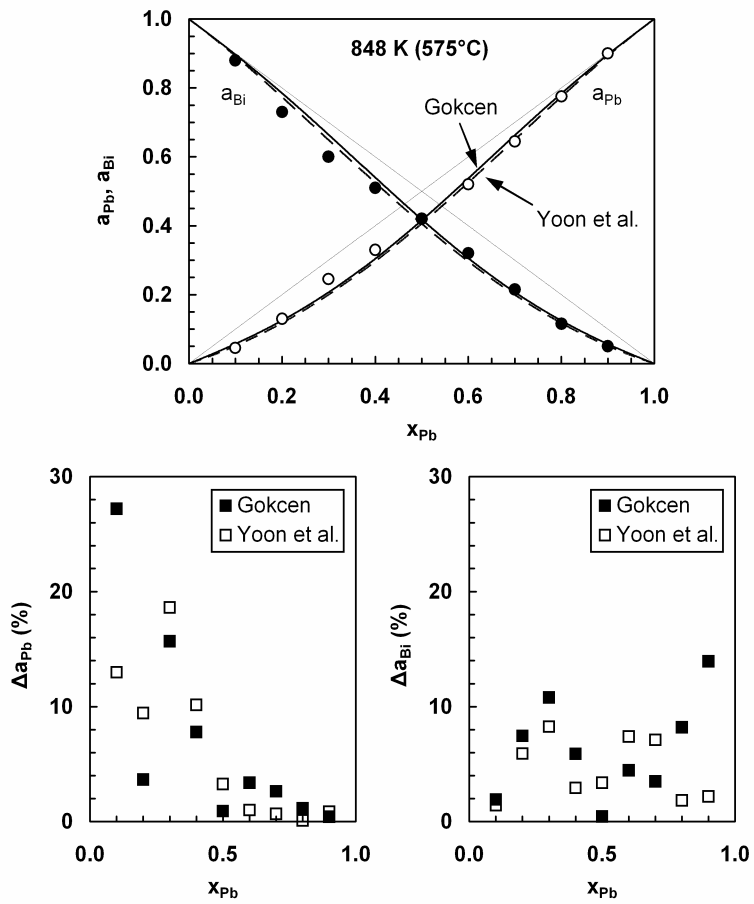


***Figure 9 –*** *Thermodynamic activities of Pb and Bi in liquid Pb-Bi alloys at 575°C calculated from the excess partial molar free energies of Pb and Bi according to Gokcen and Yoon et al., respectively, in comparison to experimental data from Agarwala et al. (open and solid circles). Bottom: Relative deviation of the calculated thermodynamic activities from the experimental data for Pb (left) and Bi (right).*

both *Gokcen* and *Yoon et al.* when they derived their equations. Fig. 6 shows such a comparison for calculated activities of Pb and Bi, $a_{Pb}$ and $a_{Bi}$, at 427°C as a function of the composition of the liquid binary alloy ($x_{Pb}$), together with experimental data published by *Roy et al.* [16]. The relative deviation of the calculated activities from the experimental data, which is also plotted in Fig. 6, indicates that the slightly higher values following from the Gokcen-equations (Eqs. (45) and (46)) correspond better with the data of *Roy et al.* than the activities resulting from the Yoon-equations (Eqs. (47) and (48)) for both Pb and Bi. The same is true when comparing activity coefficients of Pb, $\gamma_{Pb}$, calculated for liquid Pb-Bi alloys at 484°C with experimental data published by *Moser* [17] (Fig. 7). In the case of both sets of equations, the results of calculations exhibit comparatively large deviations from experimentally determined data for low Pb concentration (Fig. 7, bottom).

Analogous comparisons were performed with experimental data from *Agarwala et al.* [18], i.e., Pb and Bi activities measured at 550° and 575°C, which were published after *Gokcen* and *Yoon et al.* derived their equations and were not taken into consideration by these authors. The results for 550°C are summarised in Fig. 8, indicating that the deviation of the calculated values from the experimental data is

higher than for data which was available to *Gokcen* and *Yoon et al*. However, for $0.4 < x_{Pb} < 0.8$, the correspondence between calculation and experiment is satisfactory for both sets of equations (deviation < 10%; Fig. 8, bottom), especially when considering that experimental data can also be erroneous to some degree. The comparison with the data of *Agarwala et al.* (those for 575°C (Fig. 9) included) does not definitely show which of the two sets of equations is to be preferred as a basis for estimating the thermodynamic activity of Pb and Bi in their liquid binary alloys.

Because of the slightly better correspondence with experimental data at temperatures around 450°C, the Gokcen-equations are used to calculate thermodynamic activities of Pb and Bi in respective binary alloys. For the eutectic mixture of Pb and Bi (LBE) with $x_{Pb} = 0.45$ (corresponding to 44.8 mass% Pb) and $x_{Bi} = 0.55$ (55.2 mass% Bi), it follows that

$$a_{Pb} = \exp\left\{-0.82912 - \frac{166.80}{T/K}\right\} \tag{50}$$

and

$$a_{Bi} = \exp\left\{-0.61700 - \frac{101.79}{T/K}\right\} \tag{51}$$

The temperature-dependent values of $a_{Pb}$ and $a_{Bi}$ in LBE resulting from Eqs. (50) and (51) are plotted in Fig. 10.

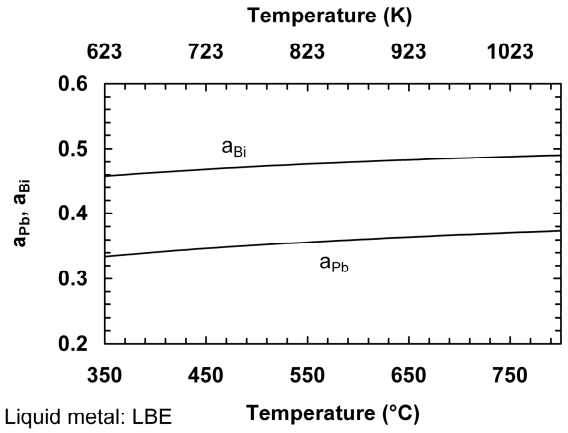


***Figure 10 –*** *Thermodynamic activities of Pb and Bi in liquid LBE as a function of temperature.*

## *4.2 Dissolution of oxygen*

In contrast to liquid Pb, there are only a few investigations regarding the dissolution of oxygen in liquid LBE published in the technical literature. Experimental data on the saturation concentration of oxygen in the interesting temperature range is

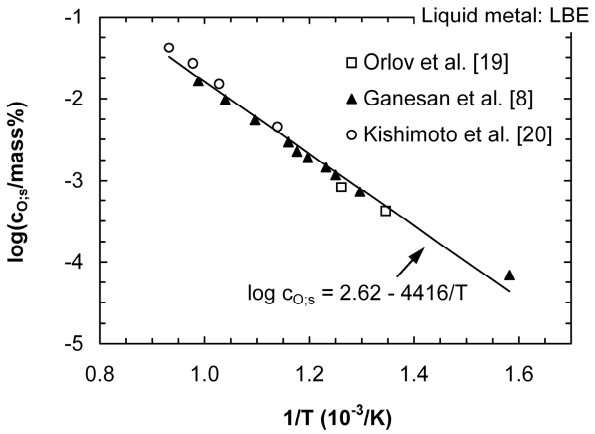


***Figure 11 –*** *Temperature-dependence of the saturation concentration of oxygen in liquid LBE.*

known from *Orlov et al.* [19] (470°C, 520°C), *Ganesan et al.* [8] (360°-740°C) and *Kishimoto et al.* [20] (600°-800°C) and is plotted as a function of the inverse of the thermodynamic temperature in Fig. 11. Fitting the parameters A and B of Eq. (11) to this data yields

$$\log(c_{O;s}/\,\mathrm{mass\%}) = 2.62 - \frac{4416}{T/\,\mathrm{K}} \tag{52}$$

for the temperature-dependent oxygen solubility in LBE at ≤ 800°C.

The oxygen partial pressure above oxygen-saturated LBE is determined by the oxide that precipitates first from the saturated solution, i.e., the oxide of the liquid

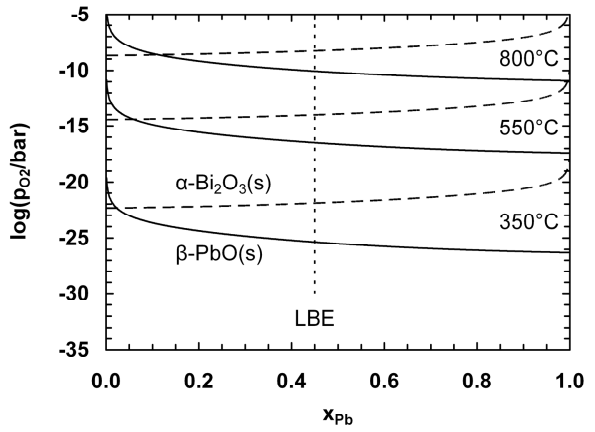


***Figure 12 –*** *Oxygen partial pressures necessary for the formation of $\alpha$-$Bi_2O_3$ and $\beta$-PbO as a function of the composition of binary Pb-Bi alloys (mole fraction of Pb) for temperatures between 350° and 800°C. The presented curves were calculated using Eq. (29), thermodynamic data for the oxides from Table 1 and activities of Pb and Bi determined on the basis of Eqs. (45) and (46).*

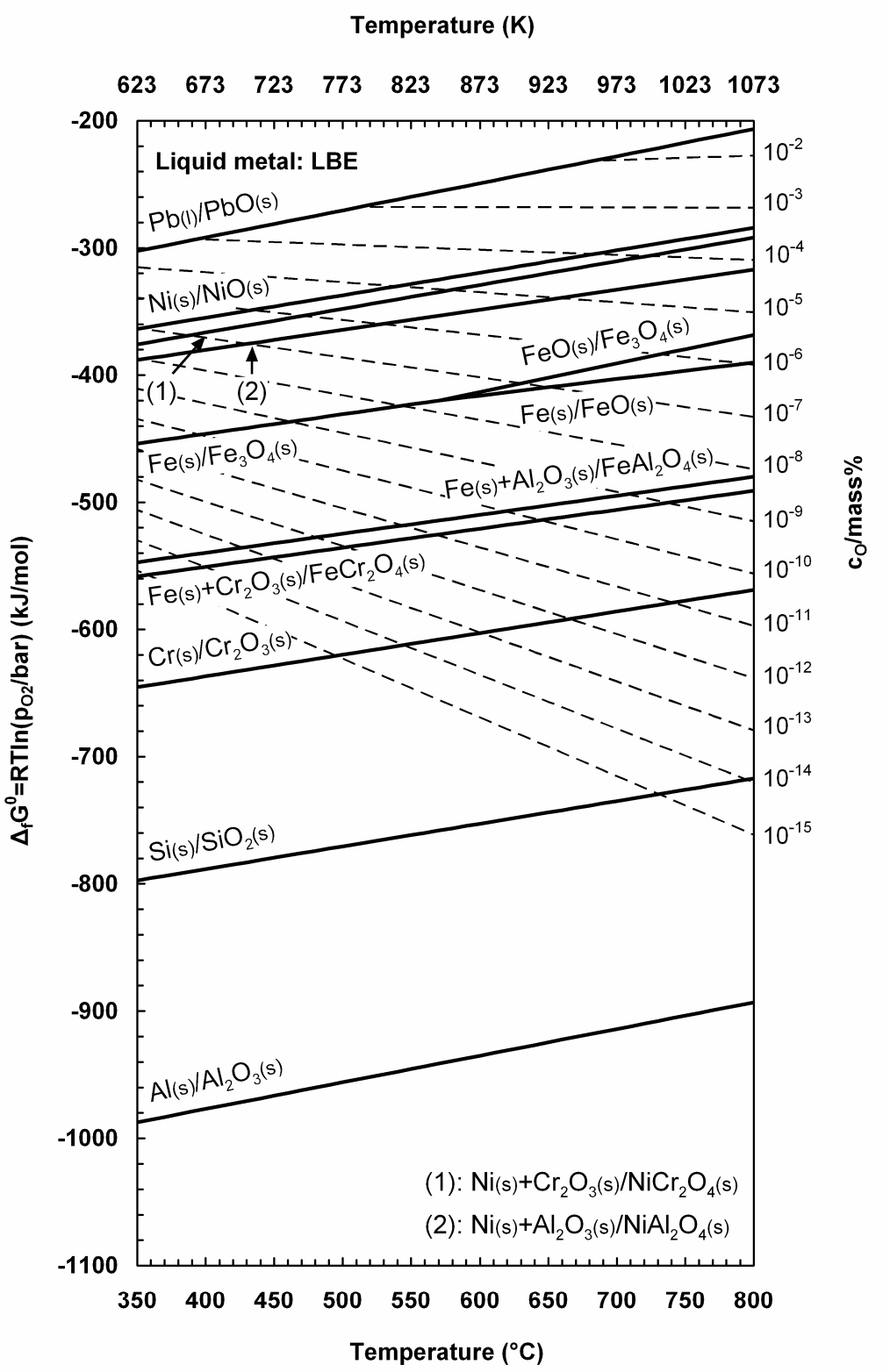


***Figure 13 –*** *Dependence of the thermodynamic stability of selected oxides of steel constituents on temperature and the concentration of oxygen dissolved in LBE.*

metal components, the formation of which needs the lowest oxygen partial pressure. According to Fig. 12, this oxide is PbO, which is corroborated by electrochemical analyses of oxygen-saturated LBE performed by *Ganesan et al.* [8]. Thus, the oxygen partial pressure above the saturated solution, $p_{O_2;s}$, can be calculated from Eq. (30) using the standard Gibbs free energy of formation of PbO listed in Table 1 and the temperature-dependent Pb activity in LBE given by Eq. (50), so that

$$p_{O_2;s} / \text{bar} = \exp\left\{25.624 - \frac{52341}{T/\text{K}}\right\} \tag{53}$$

Assuming that Sievert's law is valid for the dissolution of oxygen in LBE, the oxygen partial pressure above the unsaturated solutions follows from Eq. (15) as

$$p_{O_2} / \text{bar} = (c_O / \text{mass\%})^2 \exp\left\{13.558 - \frac{32005}{T/\text{K}}\right\} \tag{54}$$

Eq. (54) was used for the construction of the lines of constant oxygen concentration in Fig. 13.

The activity of PbO, $a_{PbO}$, in unsaturated LBE as a function of the oxygen concentration and temperature results from inserting Eq. (52) into Eq. (19), i.e.,

$$a_{PbO} = (c_O / \text{mass\%}) \exp\left\{-6.0328 + \frac{10168}{T/\text{K}}\right\} \tag{55}$$

## *4.3 Dissolution of metals and solubility products*

### *4.3.1 Iron and chromium*

The dissolution of Fe in liquid Pb-Bi alloys was studied by *Weeks et al.* [10], who determined the parameters A and B in Eq. (11) for six binary Pb-Bi alloys using experimental results at temperatures between 550° and 779°C. Values of A and B for the eutectic alloy were not presented, but can be calculated by interpolation of the available data. Doing so yields

$$\log(c_{Fe;s} / \text{mass\%}) = 2.012 - \frac{4382}{T/\text{K}} \tag{56}$$

for the temperature-dependence of the saturation concentration of Fe in liquid LBE. The saturation concentration of Cr in LBE was measured at temperatures between 400° and 550°C by *Rosenblatt et al.* [21], who approximated their experimental data by the equation

$$\log(c_{Cr;s} / \text{mass\%}) = -0.02 - \frac{2280}{T/\text{K}} \tag{57}$$

However, the single data points scatter significantly around the curve predicted by Eq. (57), which was attributed to difficulties in the chemical analysis of the small amounts of dissolved Cr and the presence of Cr oxide.

Using Eqs. (56) and (57) for $c_{Fe;s}$ and $c_{Cr;s}$, respectively, and Eq. (52) for $c_{O;s}$, the solubility products of $Fe_3O_4$, FeO and $Cr_2O_3$ in liquid LBE were calculated, i.e.,

**$Fe_3O_4$:**
$$(c_{Fe}/\text{mass\%})^3 (c_O/\text{mass\%})^4 = \exp\left\{23.745 - \frac{98459}{T/K}\right\} \quad (58)$$

**FeO:**
$$(c_{Fe}/\text{mass\%})(c_O/\text{mass\%}) = \exp\left\{5.6835 - \frac{25946}{T/K}\right\} \quad (59)$$

**$Cr_2O_3$:**
$$(c_{Cr}/\text{mass\%})^2 (c_O/\text{mass\%})^3 = \exp\left\{10.240 - \frac{98019}{T/K}\right\} \quad (60)$$

The impact of the formation of these oxides on the concentration of dissolved Fe and Cr in oxygen-containing LBE is illustrated in Fig. 14.

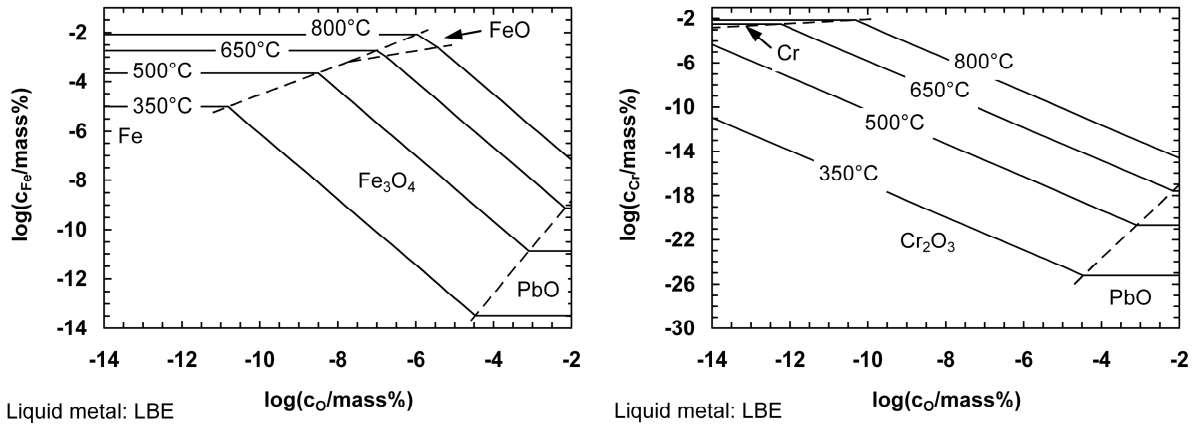


***Figure 14 –*** *Concentration of dissolved Fe (left) and Cr (right) in oxygen-containing LBE as a function of the oxygen concentration for temperatures between 350° and 800°C.*

### *4.3.2 Nickel*

The dissolution of Ni in LBE is treated separately from the other metals, as there are two stable intermetallic compounds in the binary Bi-Ni system, namely NiBi and $NiBi_3$ (Fig. 15), which are also likely to form in the case of ternary Bi-Ni-Pb alloys. The formation of intermetallic compounds limits the solubility and has to be taken into account in the correlation between the concentration of the metallic solute, $c_M$, and its activity in the liquid-metal solution, $a_M$. This can be done by either choosing the in-

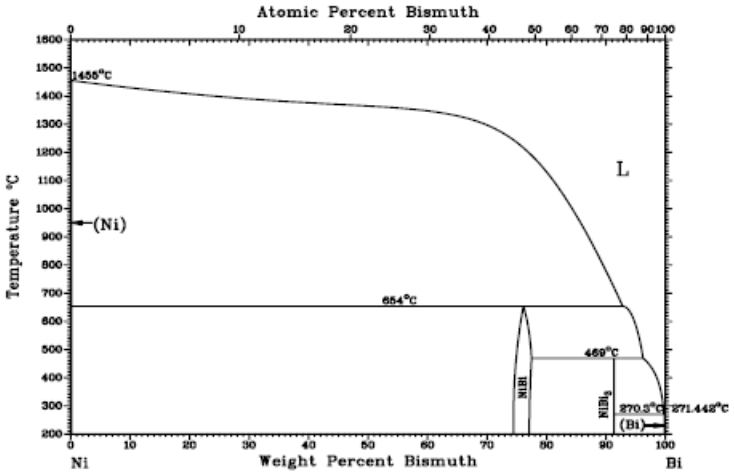


***Figure 15 –*** *Phase diagram of the binary Bi-Ni system [22].*

termetallic compound as the reference state for the chemical potential of the metallic solute, so that Eq. (9) still applies, or using the pure solid metal as the reference state (only high-melting metals are considered) and introducing the activity in the saturated solution, $a_{M;s}$, on the right hand side of Eq. (9), i.e.,

$$a_M = a_{M;s} \frac{c_M}{c_{M;s}} \tag{61}$$

In this case, $a_{M;s}$ differs from unity and corresponds to the activity of the metallic solute in the intermetallic compound (with reference to the pure solid metal). Modifications of the reference state for the chemical potential of the metallic solute or the correlation between $a_M$ and $c_M$ affect the calculation of the solubility product of respective metal oxides, i.e., Eq. (31) has to be altered accordingly when an intermetallic compound limits the solubility in the absence of oxygen. As long as the metallic solute obeys Henry's law in the liquid-metal solution, Eq. (11) can be used to approximate the temperature-dependence of the saturation concentration of the metallic solute, but the parameters A and B will change when the solid phase in equilibrium with the saturated solution changes with temperature, e.g., from the pure solid solute to an intermetallic compound.

The domains of precipitation of solid Ni, NiBi and $NiBi_3$ from Ni-saturated liquid Pb-Bi alloys are depicted in the T-$x_{Bi}$ diagram ($x_{Bi}$: mole fraction of Bi in the regarded Pb-Bi alloy) shown in Fig. 16. The boundary line between the domains of precipitation of solid Ni and NiBi was determined on the basis of thermodynamic calculations, using the standard free energy for the formation of solid NiBi from solid Ni and liquid Bi according to the chemical reaction

$$Ni_{(s)} + Bi_{(l)} \rightleftarrows NiBi_{(s)} \tag{62}$$

which can be approximated by

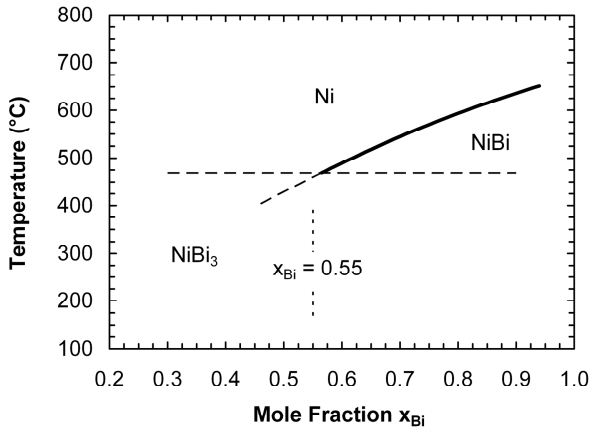


***Figure 16 –*** *Domains of precipitation of solid Ni, NiBi and $NiBi_3$ from liquid Pb-Bi alloys saturated with Ni as a function of temperature and the mole fraction of Bi in the regarded Pb-Bi alloy.*

$$\Delta_f G^0_{Ni/NiBi}/(J\,mol^{-1}) = -20384 + 21.515\,(T/K) \tag{63}$$

in the temperature range from 280° to 650°C [6]. The criterion for the precipitation of NiBi is

$$\gamma_{Bi} x_{Bi} \geq \exp\left\{\frac{\Delta_f G^0_{Ni/NiBi}}{RT}\right\} \tag{64}$$

where the activity coefficient of Bi, $\gamma_{Bi}$, was calculated from the excess partial molar free energy of Bi in binary Pb-Bi alloys (Eq. (46)). Thermodynamic data for the formation of $NiBi_3$ was not available, so that the boundaries of the domain of precipitation of $NiBi_3$ could not be calculated. As a first approximation, it was assumed that $NiBi_3$ forms at ≤ 469°C (as in the case of Ni-saturated liquid Bi), which, considering experimental findings on Ni-saturated LBE [21], is at least justified for Pb-Bi alloys with $x_{Bi} \geq 0.55$. According to Fig. 16, the Ni-containing phase that forms in equilibrium with Ni-saturated LBE at > 469°C is solid Ni. (It should be noted that neither the influence of Ni on the activity coefficient of Bi in Pb-Bi alloys nor the decrease of the molar fraction of Bi due to the dissolution of Ni were taken into account in the calculation of the boundary line between the domains of precipitation of Ni and NiBi. However, the decrease in the molar fraction of Bi shifts this boundary to lower temperatures, i.e., in the case of LBE, more significantly into the domain of precipitation of $NiBi_3$.)

Experimental data on the saturation concentration of Ni in liquid LBE was determined by *Rosenblatt et al.* [21], who approximated the temperature-dependence of the Ni solubility by the equation

$$\log(c_{Ni;s}/\,mass\%) = 1.70 - \frac{1000}{T/K} \tag{65}$$

Eq. (65) is strictly valid only in the limited temperature range of 480°-550°C, in which the solid in equilibrium with the saturated melt is solid Ni (according to Fig. 16). Thus,

Eq. (31) can be used to calculate the solubility product of NiO in this temperature range, yielding

**NiO:**
$$(c_{Ni}/\text{mass\%})(c_O/\text{mass\%}) = \exp\left\{7.7614 - \frac{14790}{T/K}\right\} \quad (66)$$

The maximum concentration of dissolved Ni as a function of the oxygen concentration following from Eqs. (65) and (66) is shown in Fig. 17, in which the curve resulting for 350°C is plotted as a dotted line, in order to indicate that these equations may only roughly approximate the concentration of dissolved Ni when $NiBi_3$ precipitates first from Ni-saturated LBE. Furthermore, the applicability of Eq. (65) (and, therefore, also the applicability of Eq. (66)) at > 550°C has to be checked experimentally, as the saturation concentration of Ni predicted by Eq. (65) is already in the range of 10 at.% at 550°C, so that at higher temperatures the saturated solutions may no longer obey Henry's law. As in the case of liquid Pb, Ni exhibits a remarkably higher solubility in liquid LBE than Fe and Cr.

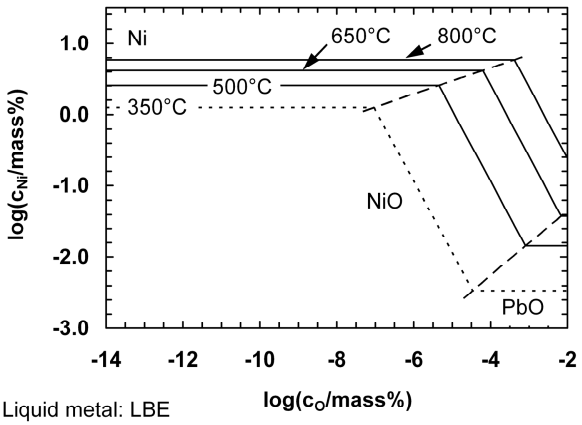


***Figure 17 –*** *Maximum concentration of Ni in oxygen-containing LBE as a function of the oxygen concentration for temperatures between 350°-800°C. The curve for 350°C does not account for the precipitation of $NiBi_3$ instead of Ni at low oxygen concentration.*

# 5 Electrochemical oxygen sensors

## *5.1 Measuring principle, sensor design and sources of error*

Electrochemical oxygen sensors measure the difference in the chemical potential of oxygen, $\mu_{O_2}$, on both sides of a solid electrolyte via the electric potential difference arising between two electric leads that transport the electrons generated or consumed at the opposing electrolyte surfaces. Necessary pre-requisites for an accurate measurement are the practically exclusive conduction of oxygen ions ($O^{2-}$) in the electrolyte and the absence of an electric current, i.e., the electric potential difference has to be recorded using a high-resistance voltmeter or a compensation method. Appropriate electrolyte materials are based on cubic zirconia ($\gamma$-$ZrO_2$), which

is partially or fully stabilised by additions of other oxides like calcia (CaO), magnesia (MgO) or yttria ($Y_2O_3$). However, the appropriateness depends on the operating conditions of the sensor, as the $O^{2-}$ and electron conductivity in these materials may change with temperature and the oxygen activity in the surrounding atmosphere. If the oxygen chemical potential on one side of the electrolyte is known (reference electrode), the chemical potential and therefore the oxygen activity and concentration on the other side can be calculated from the sensor output which, in the ideal case, corresponds to the electromotive force (EMF) of the galvanic cell formed by the sensor and the measured system.

A simple galvanic cell that describes the oxygen sensor and the measured system is

$$\text{Lead 1, } O_2(g)\ (\mu_{O_2}) \mid \text{Electrolyte} \mid O_2(g)\ (\mu_{O_2;\text{Ref}}),\ \text{Lead 2} \qquad \text{(I)}$$

where the right hand side represents the reference electrode with the fixed and known oxygen potential $\mu_{O_2;\text{Ref}}$. The half-cell reaction proceeding on both sides of the electrolyte is

$$O_2(g) + 4e^-(\text{electric lead}) \rightleftarrows 2O^{2-}(\text{electrolyte}) \qquad (67)$$

i.e., on the side exhibiting the higher oxygen potential, gaseous oxygen and electrons from the electric lead are consumed and the produced $O^{2-}$-ions are transferred onto the electrolyte (cathode). On the opposite side of the electrolyte, the reverse processes take place (anode), so that the overall cell reaction is the transition of gaseous oxygen from the cathode to the anode. Assuming that the higher oxygen potential prevails at the reference electrode, the Gibbs free energy change of the cell reaction, $\Delta G_{\text{Cell (I)}}$, is

$$\Delta G_{\text{Cell (I)}} = \mu_{O_2} - \mu_{O_2;\text{Ref}} \qquad (68)$$

and the EMF of the cell, $E_{\text{Cell (I)}}$, follows as

$$E_{\text{Cell (I)}} = -\frac{\Delta G_{\text{Cell (I)}}}{4F} = -\frac{\mu_{O_2} - \mu_{O_2;\text{Ref}}}{4F} \qquad (69)$$

where F denotes the Faraday constant. Substituting the chemical potentials of oxygen with the respective partial pressures using Eq. (4) yields

$$E_{\text{Cell (I)}} = \frac{RT}{4F} \ln \frac{p_{O_2;\text{Ref}}}{p_{O_2}} \qquad (70)$$

Because an (equilibrium) partial pressure of gaseous oxygen can be attributed to every oxygen-containing phase irrespective of the form in which oxygen is exists in this phase, Eq. (70) can be used to predict the EMF of the galvanic cell representing the oxygen sensor and the measured system even if the reference system, the measured system or both are not gaseous.

For a more detailed analysis of the output which is transmitted to a voltmeter installed between the two electric leads of Cell (I), electrochemical potentials of the involved substances have to be considered. The electrochemical potential, $\eta_i$, is defined as

$$\eta_i = \mu_i + z_i F \varphi \tag{71}$$

and represents the sum of the chemical and electric work necessary to transfer 1 mole of the electrically charged substance i (e.g., ions and electrons) to the inside of a phase where the electric potential is $\varphi$. $\mu_i$ is the chemical potential in the regarded phase and $z_i$ is the electric charge. In the case of neutral substances ($z_i = 0$), the electrochemical potential is equal to the chemical potential. Considering the half-cell reactions on both sides of the electrolyte (Eq. (67)), the electrochemical work for the formation of $O^{2-}$-ions and their transfer to the electrolyte has to be balanced by the release of electrons from the electric lead and the reaction with oxygen (cathode) and *vice versa* (anode), so that

$$\mu_{O_2;\,\mathrm{Ref}} + 4\eta_{e^-;\,\mathrm{Lead\,2}} = 2\eta_{O^{2-};\,\mathrm{Electrolyte}} \tag{72}$$

and

$$\mu_{O_2} + 4\eta_{e^-;\,\mathrm{Lead\,1}} = 2\eta_{O^{2-};\,\mathrm{Electrolyte}} \tag{73}$$

In the absence of an electric current, the electrochemical potential of $O^{2-}$-ions is constant in the electrolyte (zero driving force for $O^{2-}$ diffusion), so that combining Eqs. (72) and (73) and comparing with Eqs. (69) and (71) yields

$$E_{\mathrm{Cell\,(I)}} = \frac{\eta_{e^-;\,\mathrm{Lead\,1}} - \eta_{e^-;\,\mathrm{Lead\,2}}}{F} = -(\varphi_{\mathrm{Lead\,1}} - \varphi_{\mathrm{Lead\,2}}) + \frac{\mu_{e^-;\,\mathrm{Lead\,1}} - \mu_{e^-;\,\mathrm{Lead\,2}}}{F} \tag{74}$$

Accordingly, the difference in the electric potential between Lead 2 and Lead 1 measured with the voltmeter, i.e.,

$$E = \varphi_{\mathrm{Lead\,2}} - \varphi_{\mathrm{Lead\,1}} \tag{75}$$

coincides with the EMF of the galvanic cell, only if the difference in the chemical potential of the electrons on the right hand side of Eq. (74) vanishes. As the electrochemical potential of electrons is constant in joined electron-conducting materials in the absence of an electric current, this means that each lead may be composed of a series of such materials, but the connections to the voltmeter must be the same material. However, it should be emphasised that in the considerations up to this point temperature was regarded to be constant in the galvanic cell and along the electric leads, which is not the case for oxygen sensors under operating conditions. In practice, temperature gradients along the electric leads cannot be avoided so that, if these leads consist of different materials, thermoelectric effects may cause a deviation of the sensor output, E, from the cell EMF. In order to eliminate the resulting measuring error, either the thermoelectric voltages between the occurring pairs of electric conductors have to be determined or the sensors have to be calibrated under the designated operating conditions before use. The performance of calibration

measurements is recommended, so that other errors, e.g., potential inaccuracies in the substance data used to evaluate the sensor output, are eliminated simultaneously.

An example of an oxygen sensor developed for the use in liquid metals is schematically shown in Fig. 18. Two versions of this kind of sensor exist, the first of which works with a platinum (Pt)/air reference electrode, i.e., a stainless steel wire with a platinised tip residing in air (Fig. 18 left). The other type of sensor uses a metal/ metal-oxide pair, namely $Bi/Bi_2O_3$, and a molybdenum (Mo) wire (Fig. 18 right). In both cases, the solid electrolyte consists of stabilised zirconia which is in the form of a tube that is closed at one end. The housing of the sensor, which is part of the electric lead on the liquid-metal side of the electrolyte, is made of stainless steel and comprises the sensor head and a perforated sheath. The perforated sheath prevents the contamination of the liquid metal with fragments in the case of cracking of the ceramic tube, but allows for contact of the liquid metal with the electrolyte. The sensor head is provided with an adaptor for a bayonet-nut-connector (BNC), via which the sensor output is transmitted to a voltmeter. In the case of the Pt/air sensor, the sensor head is additionally equipped with two open tubes, in order to facilitate the ingress of air into the electrolyte tube.

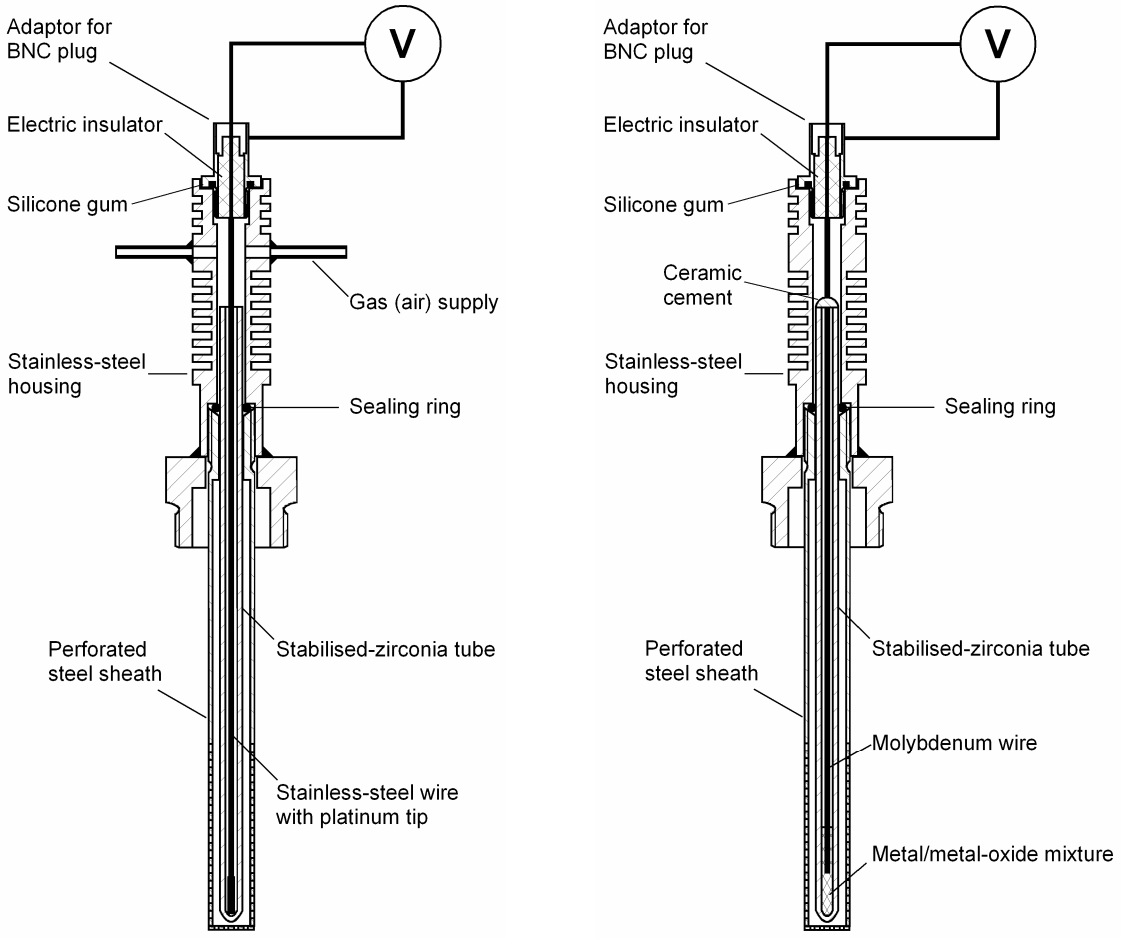


***Figure 18 –*** *Schematic illustration of oxygen sensors, which were developed for the use in liquid Pb alloys at the Forschungszentrum Karlsruhe. Left: Sensor with Pt/air reference electrode. Right: Sensor with metal/metal oxide (e.g., $Bi/Bi_2O_3$) reference system.*

The galvanic cell representing the Pt/air sensor submerged in an oxygen-containing liquid metal is

$$\text{BNC 1} \mid \text{SS} \mid \text{LM}\ (c_O) \mid ZrO_2 \mid O_{2(g)}\ (p_{O_2;\text{Ref}}),\ \text{Pt} \mid \text{SS} \mid \text{BNC 2} \qquad \text{(II)}$$

where BNC 1 and BNC 2 denote the metals forming the inner and the outer electric lead of the adaptor for the BNC, which contact the sensor housing and the electric lead inside the electrolyte tube, respectively. SS and LM stand for stainless steel and liquid metal, respectively. There are a number of junctions between different metals, with the SS/LM and SS/Pt junctions residing at the same temperature determined by the liquid metal. At the top of the sensor head, where the BNC 1/SS and BNC 2/SS junctions are located, the temperature is significantly lower, but should be the same for both junctions. Accordingly, temperature gradients within the galvanic cell occur only along the stainless steel housing on one side of the electrolyte and the stainless steel wire on the other, so that thermoelectric effects annihilate each other. In the case of the $Bi/Bi_2O_3$ sensor, which can be characterised by the galvanic cell

$$\text{BNC 1} \mid \text{SS} \mid \text{LM}\ (c_O) \mid ZrO_2 \mid Bi_{(l)}/Bi_2O_{3(s)}\ (p_{O_2;\text{Ref}}) \mid \text{Mo} \mid \text{BNC 2} \qquad \text{(III)}$$

the thermoelectric voltage between Mo and stainless steel, $E_{Mo\text{-}SS}$, adds to the theoretical cell EMF. Values for $E_{Mo\text{-}SS}$ estimated from the temperature-dependent Seebeck coefficients of Mo [23] and stainless steel (AISI 304) [24] are shown in Table 2, indicating that a measuring error caused by thermoelectric effects in the range of 3.5 mV and 12 mV can be expected for operation of the sensor at 350°C and 800°C, respectively. A less predictable error might result from interactions of Mo with the Bi-based reference system and, for both types of sensors, from the oxidation of the steel sheath in the liquid metal.

***Table 2 –*** *Estimated thermoelectric voltage for a thermocouple consisting of Mo and stainless steel (AISI 304) with the cold junction residing at 25°C*

| T/°C | 25 | 350 | 500 | 650 | 800 |
|---|---|---|---|---|---|
| $E_{Mo\text{-}SS}$/mV | 0 | 3.5 | 5.9 | 8.9 | 12.3 |

## *5.2 Evaluation of the output of Pt/air and $Bi/Bi_2O_3$ sensors*

The starting point for the evaluation of the sensor output is Eq. (70). Inserting values for the universal gas constant R (R = 8.31451 J/(mol K)) and the Faraday constant F (F = 96485.31 C/mol) yields

$$E^*/\text{V} = 2.1543 \times 10^{-5}\ \text{T/K} \ln \frac{p_{O_2;\text{Ref}}}{p_{O_2}} \qquad (75)$$

where the asterisk indicates that the equation is strictly valid only if the sensor output, E, has been corrected for thermoelectric voltages and other polarisation effects, the

occurrence of which depends on the sensor design. In the case of Pt/air sensors, the reference partial pressure is determined by the volume concentration of oxygen in air (20.946 vol.% in dry air), so that

**Pt/air:**
$$\frac{p_{O_2;\,Ref}}{p^0} = 0.20946 \tag{76}$$

The equilibrium oxygen partial pressure at a $Bi/Bi_2O_3$ reference electrode follows from Eq. (25) as

**$Bi/Bi_2O_3$:**
$$\frac{p_{O_2;\,Ref}}{p^0} = \exp\left\{23.558 - \frac{46778}{T/K}\right\} \tag{77}$$

where the data listed in Table 1 was used to calculate the standard Gibbs free energy of formation of $Bi_2O_3$. It should be noted that Eq. (77) is strictly valid only at temperatures above the melting point of Bi (271°C) and in the stability range of $\alpha$-$Bi_2O_3$ (≤ 715°C). Inserting Eq. (76) and Eq. (77), respectively, in Eq. (75) results in

**Pt/air:**
$$E^*/V = -3.3677 \times 10^{-5}\ T/K - 2.1543 \times 10^{-5}\ T/K \ln\frac{p_{O_2}}{p^0} \tag{78}$$

and

**$Bi/Bi_2O_3$:**
$$E^*/V = -1.0077 + 5.0751 \times 10^{-4}\ T/K - 2.1543 \times 10^{-5}\ T/K \ln\frac{p_{O_2}}{p^0} \tag{79}$$

from which the equilibrium oxygen partial pressure above the liquid metal was calculated, i.e.,

**Pt/air:**
$$\log\frac{p_{O_2}}{p^0} = -0.67890 - 20159\frac{E^*/V}{T/K} \tag{80}$$

**$Bi/Bi_2O_3$:**
$$\log\frac{p_{O_2}}{p^0} = 10.231 - \frac{20314}{T/K} - 20159\frac{E^*/V}{T/K} \tag{81}$$

When the dissociation partial pressure of oxides like $Fe_3O_4$ and NiO (which follows from Eq. (25) and the thermodynamic data listed in Table 1) is inserted into Eqs. (78) and (79), the resulting equations deliver the temperature dependence of the sensor output for the $Fe/Fe_3O_4$ and Ni/NiO equilibrium. Doing so yields

**Pt/air vs. $Fe/Fe_3O_4$:**
$$E^*/V = 1.4240 - 4.3192 \times 10^{-4}\ T/K \tag{82}$$

**Pt/air vs. Ni/NiO:**
$$E^*/V = 1.2275 - 4.9151 \times 10^{-4}\ T/K \tag{83}$$

**$Bi/Bi_2O_3$ vs. $Fe/Fe_3O_4$:**
$$E^*/V = 0.41627 + 1.0927 \times 10^{-4}\ T/K \tag{84}$$

**$Bi/Bi_2O_3$ vs. Ni/NiO:**
$$E^*/V = 0.21979 + 4.9678 \times 10^{-5}\ T/K \tag{85}$$

As the equilibria between solid Fe and $Fe_3O_4$ and solid Ni and NiO (and other metal/metal-oxide pairs) are easily adjusted in liquid Pb or LBE, they can be used for the calibration of oxygen sensors in these liquid metals, with Eqs. (82) to (85) providing the required reference values for the sensor output. However, the Ni/NiO equilibrium can be used for the sensor calibration in liquid LBE only at temperatures > 469°C (cf. Section 4.3.2).

*5.2.1 Lead*

The theoretical output of a Pt/air sensor as a function of temperature and oxygen mass concentration, $c_O$, in liquid Pb follows from inserting Eq. (34) into Eq. (78), which yields

**Pt/air:** $$E^*/V = 0.62880 - 2.3150\times10^{-4}\ T/K - 4.3086\times10^{-5}\ T/K \ln(c_O/\text{mass\%}) \quad (86)$$

Rearranging for the oxygen concentration and substituting the natural logarithm by the decimal logarithm results in

**Pt/air:** $$\log(c_O/\text{mass\%}) = -2.3335 + \frac{6338.1}{T/K} - 10080\frac{E^*/V}{T/K} \quad (87)$$

The relationship between the activity of lead oxide, $a_{PbO}$, in oxygen-containing liquid Pb and the sensor output was calculated using Eqs. (35) and (87), giving

**Pt/air:** $$\log a_{PbO} = -5.5435 + \frac{11438}{T/K} - 10080\frac{E^*/V}{T/K} \quad (88)$$

Inserting $a_{PbO} = 1$ and rearranging for $E^*$ yields the sensor output for oxygen-saturated Pb, i.e., the Pb/PbO equilibrium in liquid Pb:

**Pt/air vs. Pb/PbO:** $$E^*/V = 1.1347 - 5.4995\times10^{-4}\ T/K \quad (89)$$

The corresponding set of equations for $Bi/Bi_2O_3$ sensors derived from Eq. (79) is

**$Bi/Bi_2O_3$:** $$E^*/V = -0.37890 + 3.0969\times10^{-4}\ T/K - 4.3086\times10^{-5}\ T/K \ln(c_O/\text{mass\%}) \quad (90)$$

**$Bi/Bi_2O_3$:** $$\log(c_O/\text{mass\%}) = 3.1216 - \frac{3819.2}{T/K} - 10080\frac{E^*/V}{T/K} \quad (91)$$

**$Bi/Bi_2O_3$:** $$\log a_{PbO} = -0.08840 + \frac{1280.7}{T/K} - 10080\frac{E^*/V}{T/K} \quad (92)$$

**$Bi/Bi_2O_3$ vs. Pb/PbO:** $$E^*/V = 0.12705 - 8.7699\times10^{-6}\ T/K \quad (93)$$

Figs. 19 and 20 illustrate the dependence of the output on temperature and the oxygen concentration for Pt/air and $Bi/Bi_2O_3$ sensors, respectively. Additionally, the sensor output corresponding to the $Fe/Fe_3O_4$ and Ni/NiO equilibria following from Eqs. (82) to (85) is shown.

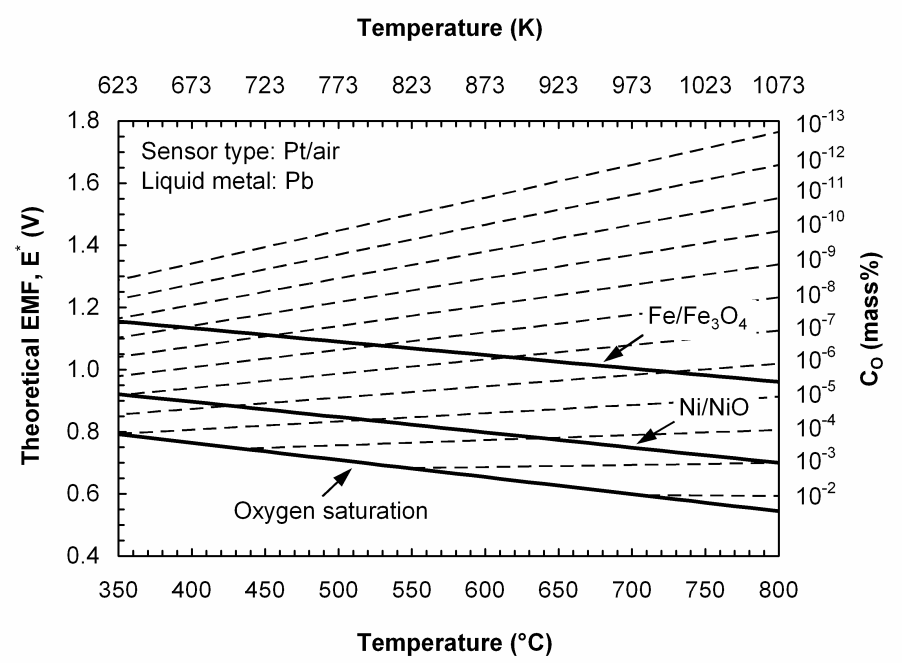


***Figure 19 –*** *Theoretical output of Pt/air sensors as a function of temperature and oxygen content of liquid Pb.*

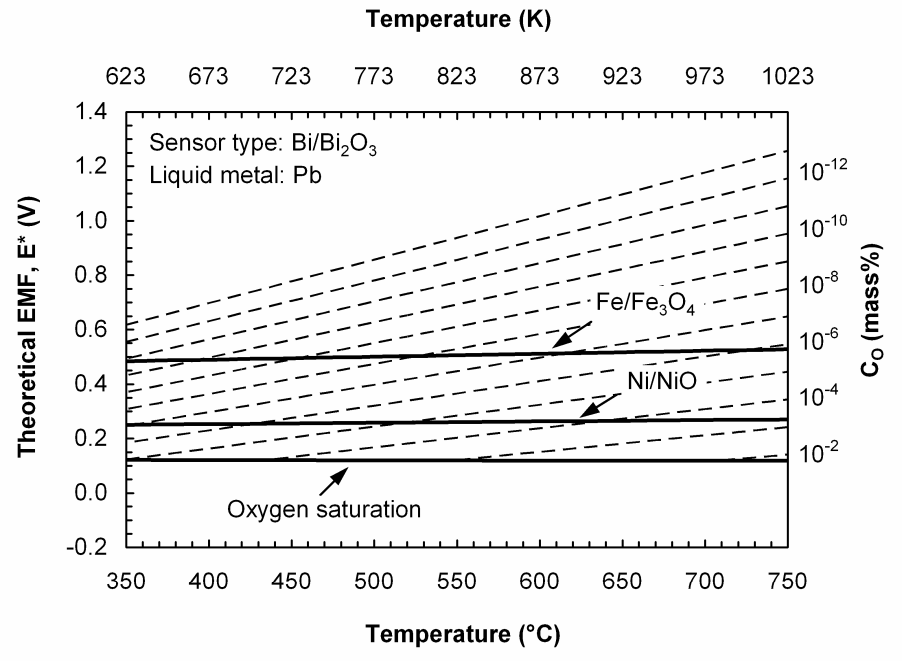


***Figure 20 –*** *Theoretical output of $Bi/Bi_2O_3$ sensors as a function of temperature and oxygen content of liquid Pb.*

*5.2.2 Lead-bismuth eutectic*

The evaluation of the output of Pt/air and $Bi/Bi_2O_3$ sensors used in LBE is analogous to the calculations for liquid Pb, with Eqs. (54) and (55) delivering the required relationship between the concentration and partial pressure of oxygen and the oxygen concentration and PbO activity, respectively. The results are:

**Pt/air:** $$E^*/V = 0.68948 - 3.2577\times10^{-4}\ T/K - 4.3086\times10^{-5}\ T/K \ln(c_O/mass\%) \quad (94)$$

**Pt/air:** $$\log(c_O/mass\%) = -3.2837 + \frac{6949.8}{T/K} - 10080\frac{E^*/V}{T/K} \quad (95)$$

**Pt/air:** $$\log a_{PbO} = -5.9037 + \frac{11366}{T/K} - 10080\frac{E^*/V}{T/K} \quad (96)$$

**Pt/air vs. Pb/PbO:** $$E^*/V = 1.1276 - 5.8568\times10^{-4}\ T/K \quad (97)$$

**$Bi/Bi_2O_3$:** $$E^*/V = -0.31822 + 2.1543\times10^{-4}\ T/K - 4.3086\times10^{-5}\ T/K \ln(c_O/mass\%) \quad (98)$$

**$Bi/Bi_2O_3$:** $$\log(c_O/mass\%) = 2.1715 - \frac{3207.5}{T/K} - 10080\frac{E^*/V}{T/K} \quad (99)$$

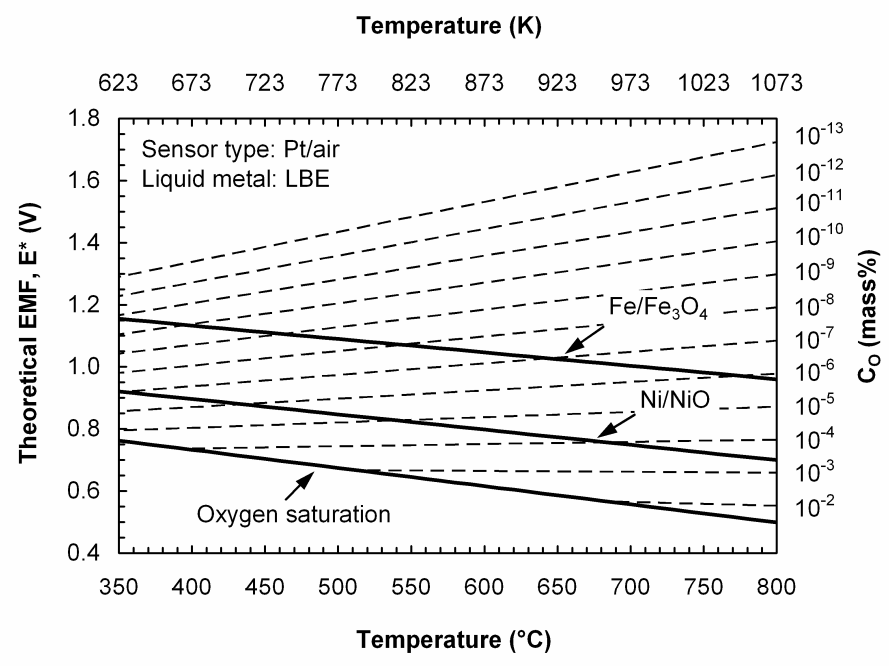


***Figure 21 –*** *Theoretical output of Pt/air sensors as a function of temperature and oxygen content of liquid LBE.*

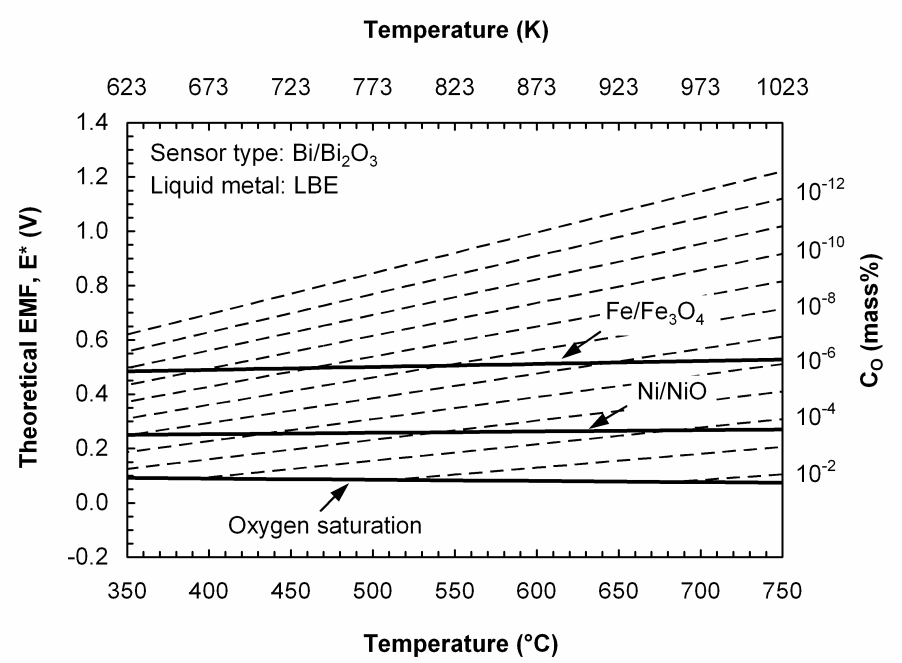


***Figure 22 –*** *Theoretical output of $Bi/Bi_2O_3$ sensors as a function of temperature and oxygen content of liquid LBE.*

**$Bi/Bi_2O_3$:**
$$\log a_{PbO} = -0.44851 + \frac{1208.4}{T/K} - 10080\frac{E^*/V}{T/K} \qquad (100)$$

**$Bi/Bi_2O_3$ vs. Pb/PbO:**
$$E^*/V = 0.11988 - 4.4495 \times 10^{-5}\ T/K \qquad (101)$$

The dependence of the output on temperature and the oxygen concentration for Pt/air and $Bi/Bi_2O_3$ sensors is shown in Figs. (21) and (22), respectively, together with the sensor output for the $Fe/Fe_3O_4$ and Ni/NiO equilibria (Eqs. (82) to (85)).

# 6 Summary

Liquid lead (Pb) and the lead-bismuth eutectic (LBE) are examples of a liquid metal that allows the reduction of steel corrosion by additions of oxygen. Favourable conditions with respect to the oxygen content follow from the comparison of the chemical potential of oxygen in the liquid metal with the oxygen potential necessary for the formation of oxides of the steel constituents, for which the diagrams presented in Fig. (2) and Fig. (13) can be used. The lines of constant oxygen concentration in these diagrams facilitate the determination of the conditions in non-isothermal plants and result from the application of Sievert's law to the dissolution of oxygen which is limited by the precipitation of lead monoxide (PbO) for both Pb and LBE. At the optimum oxygen content, oxides of steel constituents form a continuous scale on the steel surface, but precipitation of PbO does not occur at any temperature under consideration. Steel constituents that do not form solid oxides under the chosen conditions are subject to dissolution in the liquid metals as in the absence of oxygen.

The quantitative analysis of steel corrosion in oxygen-containing liquid Pb and LBE requires the correlation of the chemical potentials or activities of oxygen and the steel constituents with the respective concentrations in the liquid metal. For solvents in dilute solutions, these correlations follow from Henry's law. If Henry's law is valid up to the saturation concentration of the solvent, the logarithm of the saturation concentration is a linear function of the inverse of the thermodynamic temperature. Considering temperatures from 350° to 800°C, the solubility data found in the technical literature indicates, that, in general, Henry's law can be applied to the dissolution of oxygen and the main constituents of steels, i.e., iron (Fe), chromium (Cr) and nickel (Ni), in liquid Pb and LBE. Only in the case of the dissolution of Ni in LBE, Henry's law may not be applicable at T > 550°C. Using the correlations between activity and concentration, the solubility products of oxides of Fe, Cr and Ni were calculated from the standard Gibbs free energy of formation of these oxides, and diagrams illustrating the dependence of the maximum concentration of dissolved Fe, Cr and Ni on the concentration of dissolved oxygen were constructed for liquid Pb (Figs. 4 and 5) and LBE (Figs. 14 and 17). These diagrams, which allow semi-quantitative conclusions on the behaviour of the steel constituents, show a very pronounced decrease of the concentration of dissolved Cr as a consequence of the high stability of chromium oxide ($Cr_2O_3$). In the case of Ni, which exhibits a significantly higher solubility in liquid Pb and LBE than Fe and Cr, the decrease of the maximum concentration due to the formation of nickel monoxide (NiO) is comparatively slight and sets in at comparatively high concentration of dissolved oxygen. The mathematical equations which describe the temperature dependence of the saturation concentrations of oxygen, Fe, Cr and Ni in liquid Pb and LBE and the solubility products of oxides are summarised in Table 3.

The measurement of the oxygen content with electrochemical (or solid-electrolyte) oxygen sensors basically relies on the transformation of the difference in the chemical potential of oxygen on both sides of a solid electrolyte into an electric potential difference between two electric leads. As the oxygen potential at the reference electrode of the sensor is known, the oxygen potential in the measured system, e.g., the liquid metal, can be calculated from the sensor output. Measuring errors depending on the sensor design may result from thermoelectric effects between different materials used for the electric leads and have to be eliminated either by correcting the sensor output for known thermoelectric voltages or by calibration measurements. The dependence of the (theoretical) output of sensors working with platinum (Pt)/air or bismuth (Bi)/bismuth oxide ($Bi_2O_3$) as reference system on the oxygen concentration and temperature is depicted in Figs. 19 and 20 for liquid Pb and Figs. 21 and 22 for LBE. The mathematical equations for the evaluation of the output of these sensors are listed in Table 3.

***Table 3 –*** *Selection of equations which were presented in this report and can be used in the temperature range from 350° to 800°C, unless otherwise noted*

| | **Lead** | | **LBE** | |
|---|---|---|---|---|
| Saturation concentrations: $\log(c_{i;s}/\text{mass\%}) = A + \frac{B}{T/K}$ | | | | |
| | A | B | A | B |
| O | 3.21 | – 5100 | 2.62 | – 4416 |
| Fe | 1.824 | – 4860 | 2.012 | – 4382 |
| Cr | 3.88 | – 6949 | – 0.02 | – 2280 |
| Ni | 1.30 | – 1381 | 1.7 † | – 1000 † |
| Solubility product of oxide $Me_yO_z$: $(c_{Me}/\text{mass\%})^y (c_O/\text{mass\%})^z = \exp\left\{C + \frac{D}{T/K}\right\}$ | | | | |
| | C | D | C | D |
| $Fe_3O_4$ | 31.206 | – 107309 | 23.745 | – 98459 |
| FeO | 7.4382 | – 28455 | 5.6835 | – 25946 |
| $Cr_2O_3$ | 34.763 | – 123745 | 10.240 | – 98019 |
| NiO | 9.0280 | – 17075 | 7.7614 † | – 14790 † |
| Theoretical sensor output $E^*$: $E^*/V = C_1 + C_2 \times 10^{-4}\ T/K - 4.3086 \times 10^{-5}\ T/K \ln(c_O/\text{mass\%})$ | | | | |
| | $C_1$ | $C_2$ | $C_1$ | $C_2$ |
| Pt/air | 0.62880 | – 2.3150 | 0.68948 | – 3.2577 |
| $Bi/Bi_2O_3$ ‡ | – 0.37890 | 3.0969 | – 0.31822 | 2.1543 |
| Oxygen concentration from $E^*$: $\log(c_O/\text{mass\%}) = C_3 + \frac{C_4}{T/K} - 10080\frac{E^*/V}{T/K}$ | | | | |
| | $C_3$ | $C_4$ | $C_3$ | $C_4$ |
| Pt/air | – 2.3335 | 6338.1 | – 3.2837 | 6949.8 |
| $Bi/Bi_2O_3$ ‡ | 3.1216 | – 3819.2 | 2.1715 | – 3207.5 |

***Table 3 –*** *Continued*

| | Lead | | LBE | |
|---|---|---|---|---|
| PbO activity from $E^*$: | $\log a_{PbO} = C_5 + \frac{C_6}{T/K} - 10080\frac{E^*/V}{T/K}$ | | | |
| | $C_5$ | $C_6$ | $C_5$ | $C_6$ |
| Pt/air | – 5.5435 | 11438 | – 5.9037 | 11366 |
| $Bi/Bi_2O_3$ ‡ | – 0.0884 | 1280.7 | – 0.4485 | 1208.4 |

†: Values of the parameters strictly valid only for 469 ≤ T/°C ≤ 550

‡: Values of the parameters strictly valid for 271 ≤ T/°C ≤ 715

# References


1. L.S. Darken, R.W. Gurry, "Physical Chemistry of Metals" (New York, Toronto, London: McGraw-Hill Book Company, Inc., 1953) 259-260.

2. O.J. Kleppa, J.A. Weil, "The Solubility of Copper in Liquid Lead Below 950°C", J. Amer. Chem. Soc. 73, 10(1951) 4848-4850.

3. L.S. Darken, R.W. Gurry, "Physical Chemistry of Metals" (New York, Toronto, London: McGraw-Hill Book Company, Inc., 1953) 256-258.

4. R. Ganesan, T. Gnanasekaran, R.S. Srinivasa, "Determination of standard molar Gibbs free energy of formation of $Bi_2O_3$ over a wide temperature range by EMF method", J. Chem. Thermodynamics 35, 10(2003) 1703-1716.

5. R. Ganesan, T. Gnanasekaran, R.S. Srinivasa, "Standard molar Gibbs free energy of formation of PbO(s) over a wide temperature range from EMF measurements", J. Nucl. Mater. 320, 3(2003) 258-264.

6. HSC Chemistry® for Windows, Version 5.0, Outokumpu Research Oy (Pori, Finland, 2002).

7. D. Risold, J.-I. Nagata, R.O. Suzuki, "Thermodynamic Description of the Pb-O System", J. Phase Equilibria 19, 3(1998) 213-233.

8. R. Ganesan, T. Gnanasekaran, R.S. Srinivasa, "Diffusivity, activity and solubility of oxygen in liquid lead and lead-bismuth eutectic alloy by electrochemical methods", J. Nucl. Mater. 349, 1-2(2006) 133-149.

9. C.B. Alcock, T.N. Belford, "Thermodynamics and Solubility of Oxygen in Liquid Metals from E.M.F. Measurements Involving Solid Electrolytes. Part 1.–Lead", Trans. Faraday Soc. 60 (1964) 822-835.

10. J.R. Weeks, A.J. Romano, "Liquidus Curves and Corrosion of Fe, Ti, Zr and Cu in Liquid Bi-Pb Alloys", Corrosion-NACE 25, 3(1969) 131-136.

11. D.A. Stevenson, J. Wulff, "Liquid-Solid Phase Distribution Studies in the Systems Iron-Lead, Cobalt-Lead, Chromium-Tin and Nickel-Silver", Trans. Met. Soc. AIME 221, 4(1961) 271-275.

12. T. Alden, D.A. Stevenson, J. Wulff, "Solubility of Nickel and Chromium in Molten Lead", Trans. Met. Soc. AIME 218, 2(1958) 15-17.

13. R. Hultgren, P.D. Desai, D.T. Hawkins, M. Gleiser, K.K. Kelley, "Selected Values of the Thermodynamic Properties of Binary Alloys" (Metals Park (Ohio): The American Society for Metals, 1973) 436-445.

14. N.A. Gokcen, "The Bi-Pb (Bismuth-Lead) System", J. Phase Equilibria 13, 1(1992) 21-32.

15. S.W. Yoon, H.M. Lee, "A Thermodynamic Study of Phase Equilibria in the Sn-Bi-Pb Solder System", Calphad 22, 2(1998) 167-178.

16. P. Roy, R.L. Orr, R. Hultgren, "The Thermodynamics of Bismuth-Lead Alloys", J. Phys. Chem. 64, 8(1960) 1034-1037.

17. Z. Moser, "Thermodynamic Properties of Liquid Lead-Bismuth Solutions", Z. Metallkunde 64, 1(1973) 40-46.

18. R.C. Agarwala, V. Agarwala, A.K. Jena, "E.M.F. Cell Set-up and Thermodynamic Investigation of Liquid Pb-Bi Alloys at 550 and 575°C", Z. Metallkunde 91, 5(2000) 366-372.

19. Orlov et al. (1997). Cited by: G. Benamati, P. Buttol, C. Fazio, V. Imbeni, C. Martini, G. Palombarini, A. Rusanov, "Behaviour of different steels in liquid Pb and Pb-Bi eutectic alloy". In: "Corrosion and Oxygen Control, Minutes of the Workshop on Heavy Liquid Metal Technology, September 16-17, 1999, Forschungszentrum Karlsruhe GmbH, Germany", Ed. J. Konys, Report FZKA 6389 (Forschungszentrum Karlsruhe GmbH, 1999) 93-121.

20. A. Kishimoto, A. Wada, T. Michimoto, T. Furukawa, K. Aoto, T. Oishi, "Solubility and Activity of Oxygen in Pb-Bi Melts", Mater. Trans. 47, 1(2006) 122-128.

21. G. Rosenblatt, J.R. Wilson, "The Solubilities of Several Transition Metals in Liquid Lead-Bismuth Eutectic". In: "Corrosion by Liquid Metals", Eds. J.E. Draley and J.R. Weeks (New York, London: Plenum Press, 1970) 469-477.

22. "Binary Alloy Phase Diagrams", Electronic release (Materials Park (Ohio): ASM International, 1996).

23. N. Cusack, P. Kendall, "The Absolute Scale of Thermoelectric Power at High Temperature", Proc. Phys. Soc. (Lond.) 72, 5(1958) 898-901.

24. R.S. Graves, T.G. Kollie, D.L. McElroy, K.E. Gilchrist, "The Thermal Conductivity of AISI 304L Stainless Steel", Intern. J. Thermophys. 12, 2(1991) 409-415.